THERMAL EXPANSION IN $CUK_2Cl_4 \cdot 2H_2O$ NEAR THE CURIE TEMPERATURE

By

JOSEPH WESLEY PHILP

A DISSERTATION PRESENTED TO THE GRADUATE COUNCIL OF
THE UNIVERSITY OF FLORIDA
IN PARTIAL FULFILLMENT OF THE REQUIREMENTS FOR THE
DEGREE OF DOCTOR OF PHILOSOPHY

UNIVERSITY OF FLORIDA

1969

ACKNOWLEDGMENTS

The author would like to express his appreciation for help and guidance during the course of this work to the following persons:

Dr. E. D. Adams, who has provided aid in all phases of the research;

Dr. R. Gonano, who helped with earlier experiments. His assistance with developing the techniques used in the present work has been invaluable;

Dr. T. A. Scott, who has offered helpful suggestions:

Dr. G. C. Straty, who built the cryostat used in this experiment. The ease with which this equipment was adapted for the present project is a tribute to his ability;

Drs. D. C. Heberlein, P. N. Henriksen, M. F. Panczyk, and R. A. Scribner, whose assistance and suggestions have been valuable;

Dr. George S. Dixon, who furnished the sample upon which our measurements were made;

Mr. B. McDowell, who produced the liquid helium used.

The author is grateful to his wife, Lyla, who, although having nothing to do with the research, has helped make life more pleasant; and to his parents, Mr. & Mrs. Joseph M. Philp, who have always provided help and encouragement.

TABLE OF CONTENTS

LIST OF TABLES

LIST OF FIGURES

Figure No. Page No.

LIST OF FIGURES (cont'd.)

CHAPTER I

INTRODUCTION

Phase Change and the Critical Point

Phase changes are common occurrences in matter. Examples are the melting of ice, the evaporation of water, and the sublimation of CO_2. These changes occur slowly and in small portions of the substance. On the other hand, the domain magnetization of iron slowly decreases as the temperature is increased, until, at a temperature of 1043 F, the magnetization suddenly vanishes. This transition is due to the disappearance of long range ordering of the spin magnetic moment of the 3d electrons.

The transition in iron is an example of a phase transition brought about by the mutual cooperative interaction of many particles. Other examples include the critical point of liquid-vapor transitions, the Néel point of antiferromagnets, and the lambda-point in liquid helium. All of these are characterized by an order parameter describing the cooperative effects which increases rapidly below a critical temperature. Several such systems are listed in Table 1. taken from Kadanoff, et al.,[1] and Huang.[2]

A ferromagnet is characterized by the parallel alignment of the spins of the magnetic ions below a critical or Curie temperature, T_c. Thermal agitation randomizes the spins at temperatures above the Curie

Table 1. Cooperative Systems and the Corresponding Order Parameters

System	Order Parameter
liquid - gas[a]	density
ferromagnet[a]	domain magnetization
antiferromagnet[a]	sublattice magnetization
superconductor[a]	complex gap parameter
superfluid[a]	condensate wave function
ferroelectric[a]	lattice polarization
phase separation[a]	concentration
binary alloy (bcc)[b]	2x (number of similar nearest neighbors) + (number of dissimilar nearest neighbors)

[a]Reference 1.

[b]Reference 2.

point, but short-range ordering persists. Below the transition, however, a long-range order exists and the crystal exhibits a net magnetization over a macroscopic volume called a domain.

Where ferromagnetic ordering is increasing most rapidly, we find a large specific heat and, as we shall see later, a rapid length change. The existence of short-range order immediately above the transition is shown dramatically by the large specific heat in this region. For transitions which occur at low temperatures where nonmagnetic effects are negligible, the effects of ordering are observed to about $10T_c$. At temperatures much less than T_c, on the other hand, the few deviations from perfect ordering may be described by "spin waves" which give rise to a small specific heat.

Observations On Insulating Ferromagnets

As the experiment to be described in Chapter IV concerns an observation on a ferromagnetic salt, it is useful to briefly review the available information relating to similar materials.

There are but a few known ferromagnetic insulators. In most cases comparison with the theory is difficult. For example, gadolinium trichloride, with a Curie temperature of 2.2 K, has large dipolar interactions in addition to exchange.[3] The same is true for dysprosium ethyl sulphate which has a Curie temperature of 0.13 K, so the exchange effects are masked.[4] Several workers have studied chromium tribromide[5,6] but the specific heat anomaly at 37 K is difficult to interpret because of the large lattice contribution.

Detailed studies have been made of EuO (T_c = 69 K) and EuS (T_c = 16 K). Both have cubic, nearly ideal Heisenberg lattices and the Eu^{++} ion has spin

1/2. The susceptibility[7-9] and magnetization[10,11] have been measured. In addition, for EuO, the low-temperature anisotropy field,[12] specific heat,[13-16] thermal expansion coefficient,[17] and induced magnetostriction[18] are known. Callen and Callen[19] have applied the two-particle cluster approximation to EuO and EuS. Isotropic Heisenberg correlations are assumed for nearest and second-nearest neighbors only. The theory is successful over a wide temperature range on both sides of the transition.

Salts with the general formula $Cu(M^+)_2(X^-)_4 \cdot 2H_2O$, where M^+ is K^+, NH_4^+, or Rb^+ and X^- is Cl^- or Br^-, are ferromagnetic with Curie points at liquid helium temperatures. Miedema, <u>et al.</u>,[20] have studied $Cu(NH_4)_2Cl_4 \cdot 2H_2O$[21,22] ($T_c$ = 0.70 K), $CuRb_2Cl_4 \cdot 2H_2O$ (T_c = 1.02 K), and $Cu(NH_4)_2Br_4 \cdot 2H_2O$[23] ($T_c$ = 1.73 K) as well as $CuK_2Cl_4 \cdot 2H_2O$ (T_c = 0.88 K). They find the thermal properties of all salts are identical apart from a constant factor in the temperature. These salts crystallize in the tetragonal system with the space group D_{4h}^{14}.[24,25] The <u>c</u> axis is about 6% longer than the <u>a</u> axis (<u>a</u> axis = 7.45 Å in $CuK_2Cl_4 \cdot 2H_2O$) so the structure closely resembles body-centered cubic. Each copper ion has eight nearest and six next-nearest copper ions. The unit cell is diagrammed in Figure 1. There are two molecules in the unit cell with the copper ions at (0,0,0) and (1/2,1/2,1/2) positions. A water molecule is located on each side of the copper ion in the <u>c</u> direction. The four chlorine ions form a rhombohedron in the (001) plane about the copper ion. At room temperature, the two magnetic sites are inequivalent in the chloride salts,[26] but there is only one type of site in $Cu(NH_4)_2Br_4 \cdot 2H_2O$.[23] For the former salts, the long diagonal of the chlorine rhomboid at the cube center is perpendicular to the long diagonal at the cube edge.

The salt $CuK_2Cl_4 \cdot 2H_2O$ has been the subject of much study. Ford and

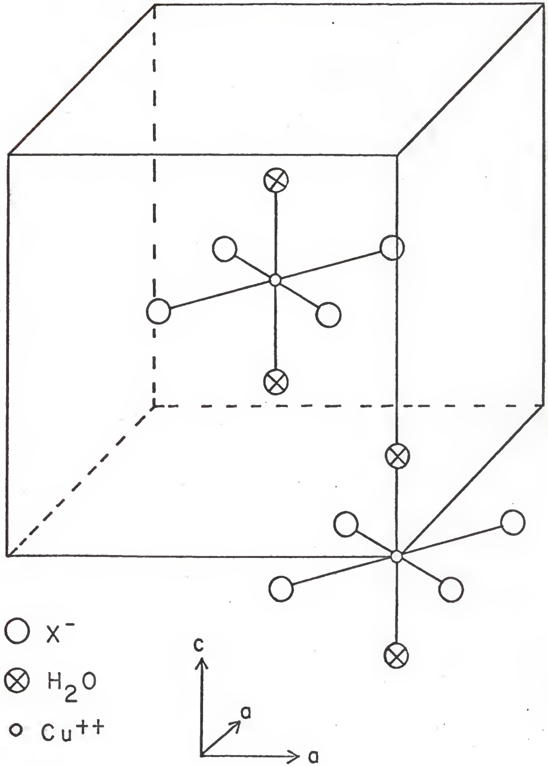

Figure 1. The Unit Cell of Salts Having the Formula $CuM_2X_4 \cdot 2H_2O$

Jeffries[27] find that, upon cooling to liquid nitrogen temperatures, perfect crystals undergo a transition which leaves all magnetic sites equivalent. They suggest the long diagonals of the chlorine rhomboids become parallel. Measurements by G. Seidel and S. H. Choh reported by Ford and Jeffries[27] suggest that the magnetic sites become equivalent because the rhomboid changes to a square.

Paramagnetic resonance absorption studies[22,26,28-31] show that the g-value is axially symmetric about the long diagonal of the chlorine rhombohedron. Paramagnetic relaxation[32] gives approximate agreement with the exchange integral found by the paramagnetic resonance measurements. The susceptibility is found to obey the Curie-Weiss law down to about 1.6 K[32] or 1.8 K.[21] The zero-field susceptibility reaches a value equal to the inverse of the demagnetizing factor in both the c and the a directions. The magnetization curves are also similar in both directions. A proton nuclear magnetic resonance study[27] shows the molecular-field model yields accurate predictions for the ratio of the magnetization to its saturation value. In addition, the anisotropy field is found to be quite small.

Miedema, et al., [20,21] find the lattice and nuclear hyperfine contributions to the specific heat are negligible in the range of measurements. The specific heat is given by

$$C/R = 0.262/T^2 \qquad T > 1.5\ \mathrm{K}$$

$$C/R = \begin{cases} -0.467 \log \epsilon + 0.43 & 10^{-3} < \epsilon < 10^{-1} \quad T < T_c \\ -0.467 \log \epsilon - 0.05 & 10^{-3} < \epsilon < 10^{-1} \quad T > T_c \end{cases}$$

where ϵ is the reduced temperature defined by $\epsilon = |T - T_c|/T_c$. In addition, the specific heat of $Cu(NH_4)_2Br_4 \cdot 2H_2O$ is described by spin

wave theory below $T = 0.5\ T_c$. This salt was chosen for low-temperature analysis as the Curie temperature is relatively high, but the same results are expected to hold for $CuK_2Cl_4 \cdot 2H_2O$.

Wood and Dalton[33] have examined several critical properties of $CuK_2Cl_4 \cdot 2H_2O$ assuming a bcc lattice with first and second-nearest neighbor Heisenberg interactions characterized by exchange parameters J_1 and J_2, respectively. It is concluded that J_2 is definitely positive (ferromagnetic interaction) and $J_2/J_1 \simeq 0.3$. The high-temperature series yield values for some critical constants shown in Table 2. Non-interacting spin-wave theory is used to reproduce fairly accurately the magnetization and specific heat below $0.4\ T_c$ using estimates of J_1 and J_2 obtained at higher temperatures. It is concluded that the exchange parameters are given by

$$J_1/k = 0.28 \pm 0.01\ \mathrm{K}$$

$$J_2/k = 0.056 \pm 0.003\ \mathrm{K}.$$

To summarize, we note that the four salts given above with the general formula $CuM_2X_4 \cdot 2H_2O$ give useful information for the following reasons:[20,27,33]

1. The magnetic interactions are due largely to first and second-nearest neighbor Heisenberg exchange.

2. The Curie temperatures are low enough that the lattice contribution to the specific heat and the expansion coefficient is negligible.

3. The copper ion has spin 1/2, so high-temperature expansions for the spin 1/2 model can be used.

4. The lattice is uncomplicated, and, at low temperatures, all magnetic sites are equivalent.

Subsequent chapters will consider the specific heat and the thermal

Table 2. Comparison of Experiment and Theory for Some Critical Constants of $CuK_2Cl_4 \cdot 2H_2O$

Property	Experiment	Theory[a]
T_c	0.88	0.85
Curie-Weiss constant	1.2 ± 0.1[b]	1.29
Energy difference between paramagnetic and ferromagnetic states at $T = 0$	5.50[c]	5.34
$C_m T^2/R$, $T > 2T_c$	2.62[c], 2.56[d]	2.36
$(S_\infty - S_c)/k$	0.222[c]	0.229
$(E_\infty - E_c)/k$	0.384[c]	0.419

[a]Reference 33.

[b]Reference 21.

[c]Reference 20.

[d]Reference 32.

expansion coefficient near the critical temperature. Unfortunately, the critical behavior of these functions is not easily determined experimentally. Many researchers note difficulty in choosing one form over another. The situation is often further clouded by corrections for lattice effects, for the shift in exchange parameters with volume, and for rounding of the lambda peak.

As noted previously, Miedema, et al.,[20,21] have found that the lattice contribution to the specific heat in $CuK_2Cl_4 \cdot 2H_2O$ is negligible over the range of their measurements (below 4.2 K). To get an order-of-magnitude estimate of the lattice contribution to the thermal expansion coefficient, α_1, assume a Gruneisen behavior for the lattice so that

$$\alpha_1 = \frac{\gamma_1 K C_1}{3V},$$

where

$$\gamma_1 = -\frac{d \log \theta}{d \log V}$$

and where θ is the Debye temperature. Assume $\gamma_1 \sim 1$ as in the alkali halides for which the expansion coefficients have been measured at low temperatures.[34] Assume also that a similar relation holds for the magnetic contribution to the thermal expansion coefficient, α_m, as in the model of Argyle, et al.,[17] described in Chapter II. Assume also that

$$\gamma_m = -\frac{d \log J}{d \log V} = 10/3$$

as suggested by Bloch[35] for systems coupled by superexchange interactions. Then

$$\frac{\alpha_1}{\alpha_m} = \frac{\gamma_1}{\gamma_m} \frac{C_1}{C_m} < \frac{C_1}{C_m} .$$

It is thus reasonable to expect that the lattice contribution is negligible in the thermal expansion coefficient as well as in the specific heat of $CuK_2Cl_4 \cdot 2H_2O$ below 4.2 K.

The shift of the exchange parameters with volume may be most simply expressed as a shift of the effective Curie point with temperature as follows:

$$\Delta T_c = \frac{dT_c}{dV} \Delta V$$

$$= T_c \; \beta \frac{d \log T_c}{d \log V} \Delta T,$$

where β is the volume thermal expansion coefficient. Heller and Benedek [36] calculate a temperature-dependent Néel temperature for MnF_2.

An alternate approach to the correction for the shift of the exchange parameters with volume assumes a constant critical temperature but shifts the temperature scale slightly. Assume for definiteness a negative $\frac{d \log T_c}{d \log V}$ and a positive expansion coefficient. Then as T_c is approached from below, the sample expands and T_c decreases. For any temperature, however, the distance to the effective transition temperature is greater than $|T - T_c|$. The same result holds for $T > T_c$. Hence Yamamoto, et al.,[37] make the simplest correction and replace $|T - T_c|$ with $|T - T_c| + \Delta$.

To get an approximate value for the change of T_c in $CuK_2Cl_4 \cdot 2H_2O$, set $\frac{d \log T_c}{d \log V} = -10/3$ as before and use $\beta \sim 3\alpha \simeq 1.5 \times 10^{-5} K^{-1} |\log \epsilon|$ near T_c.

Then $\Delta T_c \simeq 0.2 \; \mu K$ when $\epsilon = 10^{-3}$

and $\Delta T_c \simeq 8 \; \mu K$ when $\epsilon = 10^{-1}$.

A shift of this magnitude is not significant as we know T_c only to 1 mK.

Cadieu and Douglass[38] define the supercritical region as the temperature range near T_c for which the temperature-dependent coherence length is comparable with the spin-fluctuation mean free path. The supercritical behavior begins at a temperature for which the correlation length describing the spin fluctuation spectrum becomes comparable with the mean free path corresponding to some process which tends to destroy ordering. Let ϵ_s be the reduced temperature giving the onset of the supercritical region. Cadieu and Douglass find for Gd, with T_c = 292 K,

$$\epsilon_s^{-0.72} = \text{constant} \times \Gamma^{-1},$$

where Γ is an indicator of impurity. Teaney[15] has attributed the severe rounding of the specific heat anomaly of EuO to the presence of filamentary inclusions of tantalum metal.

Domb[39,40] has undertaken a comparison of graphs which contribute to the partition function of an infinite assembly and a finite assembly wrapped on a torus. This leads to an estimate of the specific heat of finite two- and three-dimensional Ising models. The reduced temperature at which the specific heat reaches a finite maximum is given by M^{-1} where the cubic assembly has M^3 spins. An order-of-magnitude estimate of ϵ_s is therefore given by

$$\epsilon_s \sim N^{-1/3},$$

where N is the number of magnetic ions in the assembly.

After corrections for the lattice effects and for the volume shift of the Curie point have been made, a form is sought to describe the specific heat or expansion coefficient outside the supercritical region (if one is observed).

Teaney[15] reports that preliminary analysis of the specific heat of EuO suggests a logarithmic dependence so that

$$C_{\pm} = A_{\pm} \log \epsilon + B_{\pm},$$

where (+) and (-) refer to the critical region above and below the transition respectively.

Yamamoto, et al.,[37] have analyzed a number of antiferromagnets as well as ferromagnetic Sm, Tb, Gd, and β-UH_3 in terms of a "pinched logarithmic" function given by

$$C_{\pm} = A \log (\epsilon + \Delta) + B_{\pm}.$$

Unfortunately, the possibility of some other kind of singularity remains in cases other than $CoCl_2 \cdot 6H_2O$ and Tb.

Miedema, et al.,[20] studied the specific heat of $CuK_2Cl_4 \cdot 2H_2O$ in detail between 0.9 T_c and 1.1 T_c. As pointed out above, they find

$$C_{\pm} = A \log \epsilon + B_{\pm}.$$

This is consistent with the "pinched logarithmic" form since the correction for the volume dependence of T_c is quite small.

Chapter II indicates how linear thermal expansion coefficient data can shed light on certain properties of the ferromagnetic insulator. First, it is shown that the temperature derivative of certain spin correlation functions describes the expansion coefficient and the specific heat. If the specific heat is proportional to the expansion coefficient, further information may be obtained about these spin correlation functions and the stress dependence of the transition temperature. Next, thermodynamics of anisotropic materials near a lambda point suggests another method to determine the stress dependence of T_c. Finally, the

expected behavior of the thermal expansion coefficient and the specific heat is discussed.

Chapter III describes the experimental procedure and the apparatus we have used to measure the linear thermal expansion of a small crystal of ferromagnetic $CuK_2Cl_4 \cdot 2H_2O$ at liquid helium temperatures.

Chapter IV gives the method of analysis and the results of our thermal expansion coefficient measurement. It is concluded that both significant spin correlation functions have the same temperature dependence well above the transition. Furthermore, the stress dependence of the transition temperature found in two ways agrees within experimental error.

CHAPTER II

THEORY

The Magnetic State

The magnetic phenomena in solids are cooperative effects which are manifestations of correlations between magnetic ions. A series of papers by P. W. Anderson[41-43] has shed considerable information on the nature of these correlations, and the brief discussion which follows is taken from this work.

Attempts to describe the magnetic state in insulating solids lead to a paradox. Whereas interactions between magnetic ions are essential to cooperative behavior, the electrons must be localized as conduction is not observed. Suppose, for example, the magnetic ion is Cu^{++} with a single d hole. Consider a single d hole allowed to wander throughout the lattice. We may put it at the bottom of the d band. When the hole is in the vicinity of another ion, it is repelled by the Coulomb energy of the localized d hole. In dilute materials for which the energy bands are narrow, the decrease in kinetic energy is outweighed by the Coulomb correlation energy, U, so the hole remains localized.

If a solid were simply a lattice of non-overlapping free-ion wavefunctions, paramagnetic behavior would be observed at all temperatures. The interactions which lead to spin correlations are of electrostatic origin, however, and are a function of the wavefunctions of the magnetic ions and the non-magnetic ligands in the solid. Anderson has described a

perturbation procedure which allows one to discuss the magnetic effects without becoming involved in the complex problems of wavefunctions in solids.

What is desired is a procedure for separating the problem into two parts such that the part containing the magnetic interaction is not a large perturbation on the other part. The Heitler-London treatment requires that the interaction of magnetic ions with the ligands be treated as part of the perturbation. This is a much larger perturbation than the magnetic effects alone.

Assume only one d hole per magnetic site for definiteness. Suppose, with Anderson, we consider the diamagnetic lattice formed by filling the d hole in every magnetic ion but one. Adjust the nuclear potential so the single hole sees the correct potential as it moves through the lattice. This is the ligand field theory aspect of the problem and involves the complete solution of the lattice exclusive of exchange effects. The one-hole wavefunction may be a Bloch running wave orthogonalized to the magnetic ion core, but since the ligand engages in covalent bonds with the magnetic ion, the core wavefunction contains a mixture of d functions. The Bloch wave must then contain an antibonding admixture of the ligand function. This is the mechanism which gives rise to superexchange via non-magnetic ions, although this treatment shows that once the non-magnetic problem of the lattice without exchange effects is solved, the ligands need not be considered further.

Anderson has shown that the effect of the ligands can be summarized in transfer integrals $b_{nn'}(R - R')$ which allow transitions between magnetic ion sites R and R' and states n and n' without change of spin. All other effects follow from many-electron interactions.

The b integrals allow a hole to decrease its kinetic energy by making virtual transitions to other sites. This decrease in kinetic energy is given roughly by $2b^2/U$, where U is the Coulomb correlation energy discussed earlier. Clearly, the transition is only allowed if the spins at the two sites are opposite, since the b's do not cause a change in spin. Hence we can represent the energy shift by

$$4b^2/U(-1/4 + S\cdot S').$$

This is not a true exchange effect as it occurs for antiparallel spins, although it is useful to ignore this distinction and label the effect kinetic or antiferromagnetic superexchange.

Other spin-dependent inter-ion effects follow using the Hartree-Fock machinery with the wavefunctions obtained from the solution of the ligand field aspect of the problem. The most significant of these effects is the familiar ferromagnetic potential exchange given by

$$-J_{nn'}(R - R')(1/4 + S\cdot S'),$$

where J is the Coulomb self-energy of an "overlap charge distribution" using states n and n'.

Although other effects can be treated with the present method, antiferromagnetic kinetic exchange resulting from virtual transfer between magnetic ions and ferromagnetic Heisenberg potential exchange usually dominate in materials for which magnetic effects are due to a single d hole or electron.

One concludes that the effective Hamiltonian, H, for insulators with spins coupled by superexchange interaction is

$$H = \sum_{\substack{\text{magnetic ion} \\ \text{sites } R,\, R'}} J(R - R')\, S\cdot S'$$

where constant terms are neglected and the sign of the exchange parameters is positive or negative as kinetic or potential exchange dominates. This is the familiar Heisenberg Hamiltonian.

Spin Correlation Functions

The treatment of Anderson justifies the Heisenberg Hamiltonian for systems coupled by superexchange interactions. However, an efficacious procedure for determining the thermal expansion coefficient from this Hamiltonian must entail further assumptions as there is no exact solution of a three-dimensional Heisenberg system. A useful statement of the problem has been offered by Callen and Callen[44] who have given expressions relating the macroscopic strains to products of microscopic coupling constants and spin correlation functions. Their development includes single-ion crystal field effects and two-ion interactions. The strains are characterized entirely by three spin correlation functions: the one-ion longitudinal correlation function which varies as $\langle(S_f^z)^2\rangle$ (subscripts label magnetic ions), the two-ion isotropic correlation function which varies as $\langle S_f \cdot S_g \rangle$, and the two-ion longitudinal correlation function which varies as $\langle(S_f^z S_g^z - \frac{1}{3} S_f \cdot S_g)\rangle$.

It is useful to apply the procedure described by Callen and Callen to the tetragonal system appropriate for $CuK_2Cl_4 \cdot 2H_2O$. We assume there is no easy or preferred direction of magnetization,[21] so the magnetization within a domain is equally likely to lie in any direction. Furthermore, the one-ion longitudinal correlation function is constant for spin-1/2 systems and therefore does not contribute to the expansion coefficient. Hence the linear expansion coefficient, α, measured in a direction specified by the

unit vector $\bar{B}$ is

$$\alpha = \sum_{f,g} [K^1_{fg} + K^2_{fg} (\tfrac{1}{3} - B^2_z)] \frac{\partial}{\partial T} \langle S_f \cdot S_g \rangle +$$

$$\sum_{f,g} [K^3_{fg} B_x B_z + K^4_{fg} (B_x + B_y) B_z] \frac{\partial}{\partial T} \langle S^z_f S^z_g - \tfrac{1}{3} S_f \cdot S_g \rangle,$$

where the K's are products of elastic constants with two-ion magneto-elastic coupling coefficients. For α along the a axis, only one component of $\bar{B}$ is nonzero. We have then that

$$\alpha = \sum_{f,g} K_{fg} \frac{\partial}{\partial T} \langle S_f \cdot S_g \rangle.$$

Since all magnetic sites are equivalent and first- and second-nearest neighbors dominate the interaction, the sum has only two terms:

$$\alpha = N z_1 K_1 \frac{\partial}{\partial T} \langle S_1 \cdot S_2 \rangle + N z_2 K_2 \frac{\partial}{\partial T} \langle S_1 \cdot S_3 \rangle, \qquad [1]$$

where N is the number of ions per unit volume, z_1 is the number of nearest neighbors ($z_1 = 8$), z_2 is the number of next-nearest neighbors ($z_2 = 6$), and ions two and three are representative nearest and next-nearest neighbors of ion one.

Since the K's are functions of the stresses only, Eq. [1] is derivable from a Gibbs free energy given by

$$G = J_1 g_1(J_1/T) + J_2 g_2(J_2/T),$$

with

$$K_1 = -\frac{1}{V} \frac{\partial J_1}{\partial \sigma},$$

and

$$K_2 = -\frac{1}{V} \frac{\partial J_2}{\partial \sigma},$$

and where σ is the component of stress in the a direction, V is the molar

volume, and the exchange parameters are functions of the stresses only. Then finally we have

$$\alpha = -\frac{Nz_1}{V}\frac{\partial J_1}{\partial\sigma}\frac{\partial}{\partial T}\langle S_1\cdot S_2\rangle - \frac{Nz_2}{V}\frac{\partial J_2}{\partial\sigma}\frac{\partial}{\partial T}\langle S_1\cdot S_3\rangle. \qquad [2]$$

It is interesting that the magnetic contribution to the specific heat at constant stress, C_σ, is given by

$$C_\sigma = Nz_1J_1\frac{\partial}{\partial T}\langle S_1\cdot S_2\rangle + Nz_2J_2\frac{\partial}{\partial T}\langle S_1\cdot S_3\rangle. \qquad [3]$$

Suppose that the a axis linear expansion coefficient and the constant-stress specific heat are found to be proportional. Let $P = V\,\alpha/C_\sigma$. Then one or both of the following is true:

1. $$P = \frac{\partial \ln J_1}{\partial\sigma} = \frac{\partial \ln J_2}{\partial\sigma}$$

$$= \frac{\partial\,[\ln(z_1 + rz_2) + \ln J_1]}{\partial\sigma} = \frac{\partial \ln\,(z_1J_1 + z_2J_2)}{\partial\sigma}$$

where $r = J_2/J_1$ (about 0.3 for $CuK_2Cl_4\cdot 2H_2O$).[33] We assume the transition temperature scales with the interaction energy. Then we have

$$P = \frac{\partial \ln T_c}{\partial\sigma}. \qquad [4]$$

2. The two spin correlation functions have proportional temperature derivatives. In this case, let

$$\frac{\partial}{\partial T}\langle S_1\cdot S_3\rangle = M\frac{\partial}{\partial T}\langle S_1\cdot S_2\rangle,$$

where M is a constant. Then

$$P = \frac{\partial \ln(z_1J_1 + Mz_2J_2)}{\partial\sigma} .$$

Callen and Callen have applied cluster approximation methods to find that the correlation functions have approximately equal temperature derivatives above $T_c/5$.[19] These calculations are not expected to apply in the critical region, but they suggest that well above the transition $M = 1$ so that

$$P = \frac{\partial \ln T_c}{\partial\sigma} . \qquad [5]$$

Thermodynamics

It is necessary to prelude the study of the thermodynamics of the lambda transition with a discussion of the critical behavior of the compressibility. The model we use is not adequate for $CuK_2Cl_4 \cdot 2H_2O$, but order-of-magnitude results are sufficient to show that the compressibility is constant. Then the thermodynamics of anisotropic media near a critical point can be applied to suggest another method to determine $\frac{\partial T_c}{\partial\sigma}$. A formula will also be derived for the shift of the Curie point with strain.

Argyle, Miyata, and Schultz[17] have considered a model which assumes the Hamiltonian is the sum of a Gruneisen lattice term plus a magnetic term involving exchange constants which all exhibit the same volume dependence. The differentiations to find the compressibility, K, give a lattice term, K_l, and a magnetic compressibility, K_m, related by

$$K = (K_m^{-1} + K_l^{-1})^{-1} = K_l(1 + K_l/K_m)^{-1} ,$$

where

$$K_m^{-1} = -T/VC_m \left(\frac{d \log J}{d \log V} \right)^2 + \text{term negligible near } T_c. \qquad [6]$$

We estimate the ratio K_1/K_m. Assume $\frac{d \log J}{d \log V}$ is approximately -10/3 as suggested by Bloch[35] for systems coupled by superexchange interactions. Reviews by Huntington[45] and Aleksandrov and Rӯzhova[46] have attempted to collect all known data on the elastic constants of crystals. The latter review is complete through 1960. Information about the compressibility of crystals similar to $CuK_2Cl_4 \cdot 2H_2O$ is seriously lacking. From the compilation of Huntington, we take a typical value for the alum salts. Hence we assume $K_1 \simeq 7 \times 10^{-12} cm^2/dyne$. In the critical region where K_m decreases most rapidly, the asymptotic part of the magnetic contribution to the specific heat is[20] $0.467R|\log \epsilon|$. In this crude approximation, we use Eq. [6] to find

$$K_1/K_m = -1 \qquad \text{when } \epsilon \sim 10^{-50000}.$$

and

$$K_1/K_m = -10^{-4} \qquad \text{when } \epsilon \sim 10^{-4}.$$

This result has two consequences.

1. The compressibility may be considered constant and equal to that measured away from the critical region.

2. A more fundamental consequence concerns the nature of the transition, for when $|K_1/K_m| > 1$, the total compressibility is negative. This leads to a first-order transition.[47] The finite size of the magnetic domain will limit the divergence of the specific heat even in perfect crystals when the reduced temperature is on the order of 10^{-6}.[39] Hence, the lambda nature of the transition is preserved.

Janovec[48] has extended to anisotropic dielectrics the Buckingham and

Fairbank[49] treatment of the thermodynamics of the lambda transition. To proceed with an analogous development for ferromagnets,[50] a relation among partial derivatives is needed.

Suppose W is a function of seven of the eight variables y,z, and x_i, where i = 1,...,6. Let us adopt the following conventions:

1. Use x to represent the set of six variables x_i, i = 1,...,6.

2. Use $x_{j/i}$ to represent the set of five variables x_j, j = 1,...,6, except $j \neq i$.

Then

$$dW = \sum_k \left(\frac{\partial W}{\partial x_k}\right)_{x_{j/k},y} dx_k + \left(\frac{\partial W}{\partial y}\right)_x dy$$

or

$$dW = \left(\frac{\partial W}{\partial y}\right)_{x_{j/i},z} dy + \left(\frac{\partial W}{\partial z}\right)_{x_{j/i},y} dz + \sum_{k\neq i}\left(\frac{\partial W}{\partial x_k}\right)_{x_{j/i,k}\,y,z} dx_k .$$

Considering

$$x_i = x_i(x_{j/i},y,z),$$

$$dx_i = \sum_{k\neq i}\left(\frac{\partial x_i}{\partial x_k}\right)_{x_{j/i,k},y,z} dx_k + \left(\frac{\partial x_i}{\partial y}\right)_{x_{j/i},z} dy + \left(\frac{\partial x_i}{\partial z}\right)_{x_{j/i},y} dz.$$

Equating the value of dW and setting d_z = o and $dx_{j/i}$ = o, we find the following identity:

$$\left(\frac{\partial W}{\partial y}\right)_x = \left(\frac{\partial W}{\partial y}\right)_{x_{j/i},z} - \left(\frac{\partial W}{\partial_{x_i}}\right)_{x_{j/i},y}\left(\frac{\partial x_i}{\partial y}\right)_{x_{j/i},z} . \qquad [7]$$

It is useful to introduce the "neighborhood temperature," t, given by

$T - T_c$. The properties of t are discussed by Buckingham and Fairbank. We will consider T_c a function of the stresses only.

The specific heat at zero stress is

$$C_\sigma = T\left(\frac{\partial s}{\partial T}\right)_\sigma .$$

Using Eq. [7], we find

$$\left(\frac{\partial s}{\partial T}\right)_\sigma = \left(\frac{\partial s}{\partial T}\right)_{\sigma_{j/i},t} - \left(\frac{\partial s}{\partial \sigma_i}\right)_{\sigma_{j/i},T} \left(\frac{\partial \sigma_i}{\partial T}\right)_{\sigma_{j/i},t} ,$$

so that we have for all temperatures

$$C_\sigma = T\left(\frac{\partial s}{\partial T_c}\right)_{\sigma_{j/i},t} - TV\alpha_i \left(\frac{\partial T_c}{\partial \sigma_i}\right)^{-1}_{\sigma_{j/i}} , \qquad [8]$$

where

$$\alpha_i = \left(\frac{\partial e_i}{\partial T}\right)_\sigma$$

and e_i is the strain function.

Assuming the shape of the transition is not a strong function of stress, the rate of change in entropy with respect to stress at a distance t from the transition is small. Since T_c is a function of stress only, neither is the rate of entropy change with respect to T_c large. Hence $T\left(\frac{\partial s}{\partial T_c}\right)_t$ is small and constant compared with the large and rapidly varying expansion coefficient and specific heat. Thus, to a good approximation,

$$C_\sigma = \text{constant} - T_c V\alpha_i \left(\frac{\partial T_c}{\partial \sigma}\right)^{-1}_{\sigma_{j/i}} \quad \text{near } T_c . \qquad [9]$$

The constant of proportionality between the asymptotic parts of the specific heat and the linear expansion coefficient gives the stress dependence of the transition temperature.

The dependence of the transition temperature on the strains is of interest. We use Eq. [7] again to find

$$\left(\frac{\partial e_i}{\partial T}\right)_\sigma = \left(\frac{\partial e_i}{\partial T}\right)_{\sigma_{j/i},t} - \left(\frac{\partial e_i}{\partial \sigma_i}\right)_{\sigma_{j/i},T} \left(\frac{\partial \sigma_i}{\partial T}\right)_{\sigma_{j/i},t}$$

or

$$\alpha_i = \left(\frac{\partial T_c}{\partial e_i}\right)^{-1}_{\sigma_{j/i},t} - s_{ii} \left(\frac{\partial T_c}{\partial \sigma_i}\right)^{-1}_{\sigma_{j/i}},$$

where the s_{ki} are the moduli of compliance for the crystal given by

$$s_{ki} = \left(\frac{\partial e_k}{\partial \sigma_i}\right)_{\sigma_{j/i},T} .$$

Let us estimate the value of each term in this relation. First, we find

$$\left(\frac{\partial T_c}{\partial e_i}\right)^{-1}_{\sigma_{j/i},t} = \frac{1}{3T_c}\left(\frac{d \log T_c}{d \log V}\right)^{-1}$$

for isotropic materials. Assume

$$\frac{d \log T_c}{d \log V} \simeq - \frac{10}{3}$$

as suggested by Bloch.[35] Then we have

$$\left(\frac{\partial T_c}{\partial e_i}\right)^{-1}_{\sigma_{j/i},t} \sim - 0.1 \ K^{-1}.$$

Take as an order-of-magnitude estimate for s_{ii} the room temperature compressibility of alum[45] divided by three. Our measurements indicate

$$\left(\frac{\partial T_c}{\partial \sigma_i}\right)_{\sigma_{j/i}} = -\ 1.5\times10^{-11}\mathrm{K\ cm^2/dyne}$$

for the a direction, so we estimate

$$s_{ii}\left(\frac{\partial T_c}{\partial \sigma_i}\right)^{-1}_{\sigma_{j/i}} \sim -0.2\mathrm{K}^{-1}\ .$$

The asymptotic value of α in the a direction is about $5\times10^{-6}\mathrm{K}^{-1}|\log\epsilon|$, so over the range of measurements,

$$\alpha < 3\times10^{-5}\mathrm{K}^{-1}.$$

Hence α_i may be neglected with respect to the other terms and we have

$$\left(\frac{\partial T_c}{\partial e_i}\right)_{\sigma_{j/i},t} = \frac{1}{s_{ii}}\left(\frac{\partial T_c}{\partial \sigma_i}\right)_{\sigma_{j/i}} \quad . \qquad [10]$$

Eq. [10] gives the dependence of the interaction energy (proportional to T_c) on the lattice parameters. These quantities can be computed from the less interesting stress dependences of the transition temperature only if the moduli of compliance are known. It is unfortunate that these are not available for any salts having the general formula $CuM_2X_4 \cdot 2H_2O$.

Predicted Behavior of the Thermal Expansion Coefficient

It is desirable to compare the measured expansion coefficient with the behavior predicted by the theory. This comparison is possible for $CuK_2Cl_4 \cdot 2H_2O$ in three distinct temperature regions as follows:

1. The spin wave approximation has been successfully applied to the specific heat of $Cu(NH_4)_2Br_4 \cdot 2H_2O$[20] at temperatures below 0.5 T_c. Our data for $CuK_2Cl_4 \cdot 2H_2O$ cannot be compared with this theory as measurements do not extend to sufficiently low temperatures.

2. The magnetic contribution to the specific heat is expected[33,51] to be proportional to T^{-2} well above the Curie point. This prediction is verified by Miedema, et al.,[20] and Van den Broek, et al.[32] The argument of Callen and Callen discussed previously suggests that the expansion coefficient will vary as the specific heat in this temperature range.

3. In the critical region (reduced temperatures less than about 0.1), no form for the thermal expansion coefficient is predicted unambiguously by the theory.

Domb has recently published a review of critical behavior of magnetic systems.[52] Numerous references to previous work appear; they will not be repeated here. Several general considerations discussed by Domb should be mentioned.

1. The critical behavior of the thermodynamic functions is more strongly influenced by the dimensionality of the system than by details of the lattice structure. For example, the Curie point of a two-dimensional Heisenberg ferromagnet is at absolute zero, while $T_c \sim J/k$ for all three-dimensional systems.

2. The behavior of the susceptibility above the transition is predicted theoretically and there is reasonable experimental verification. The specific heat is much more difficult to predict and depends more strongly on the model chosen.

3. The divergence of the specific heat above the transition is somewhat slower for Heisenberg systems than for Ising.

Domb suggests that for a Heisenberg ferromagnet with spin 1/2, the specific heat diverges slowly and may be logarithmic for all lattice structures.

Baker, <u>et al</u>.,[53] have analyzed the specific heats of several spin-1/2 Heisenberg lattices. For the bcc lattice they find

$$C = (T_c/T)^2[A - B(1 - T_c/T)^{0.20}] \quad 0.05 < \epsilon < 0.3,\ T > T_c.$$

If, however, one allows the critical temperature as determined by the specific heat to differ from that determined from the susceptibility, a logarithmic function is also reasonable.

CHAPTER III

EXPERIMENTAL PROCEDURE AND APPARATUS

The Sample

The $CuK_2Cl_4 \cdot 2H_2O$ sample upon which our thermal expansion measurements were made was prepared by Dr. George S. Dixon, Jr. at the Oak Ridge National Laboratory, who studied an adjacent section of the same crystal and found that piece to be a single crystal and of high quality. Our piece has visible faults, however.

As the saw cut on the material we received lay in the (100) plane, we chose to make our measurements perpendicular to this cut. After performing the necessary cuts with a Lastec saw using a non-abrasive wire moistened with water, the sample height was only 0.38 cm. The two faces in the (100) plane were polished by moving the crystal about on a very slightly moistened cloth stretched across a smooth surface. These faces are irregular in shape and have an area of approximately 1 cm^2.

Our experience with hydrated crystals cautions against evacuating the space around such a material at temperatures greater than 0 C. Care was exercised to see that the sample chamber was at atmospheric pressure unless it was well below the freezing point of water. Furthermore, these salts tend to deteriorate if exposed to air. We therefore stored our crystals in vacuum-pump oil.

As $CuK_2Cl_4 \cdot 2H_2O$ reacts with the copper sample chamber, 1/2 mil mylar sheets were sandwiched between the sample and the copper. These sheets are quite thin and do not affect the measurements. A coating of varnish, grease, or heavy oil might apply stress at low temperatures and was not used.

The Cryogenics

The cryostat is similar to that described by Walsh.[54] It has been described by Straty,[55] although a number of small changes have been made. Figure 2 shows the cryostat schematically. Both dewars are sealed at the top with rubber O-rings so the nitrogen can be pumped below its triple point as will be discussed later, and the helium boil-off can be recovered. The tubulation extending into the liquid helium bath enters a vacuum-tight cylinder enclosing a container of liquid He^4 (the He^4 evaporator) and another evaporator for liquid He^3. The sample chamber is attached to the He^3 evaporator and can be cooled to nearly 0.3 K.

The brass cylindrical container enclosing the evaporators and the sample chamber is attached to a flange on the cryostat stem using a vacuum-tight gasket of 0.075 cm diameter pure indium wire. After the initial liquid helium transfer, the He^4 exchange gas in this container is evacuated by pumping for several hours with a Consolidated Vacuum Corporation model PMCS-2C oil diffusion pump backed by a Welch model 1400 pump.

The He^4 evaporator is filled from the bath via a modified Hoke valve operated by a long shaft extending through the top flange of the cryostat. The evaporator temperature can be maintained at approximately 1 K for over 24 hours by pumping on the enclosed helium with a Welch model 1402 pump or a high-volume Kinney model KC-46 pump. A radiation shield attached

Figure 2. Schematic Drawing of the Cryogenics

A. Flexible stainless steel tubing for returning He^3

B. Flexible stainless steel tubing to sample chamber pump

C. Flexible stainless steel tubing to manometry system

D. Flexible stainless steel tubing to He^3 pump

E. Quick vacuum coupling for exchange gas pumping line

F. Rubber hose for He^4 evaporator pumping line

G. Rubber hose to He^4 recovery system

H. He^3 diffusion pump

I. Rubber inner tube

J. N_2 fill-pump line

K. N_2 bath

L. He^4 bath

M. He^4 evaporator

N. Radiation shield

O. He^3 evaporator

P. Sample chamber exchange gas container

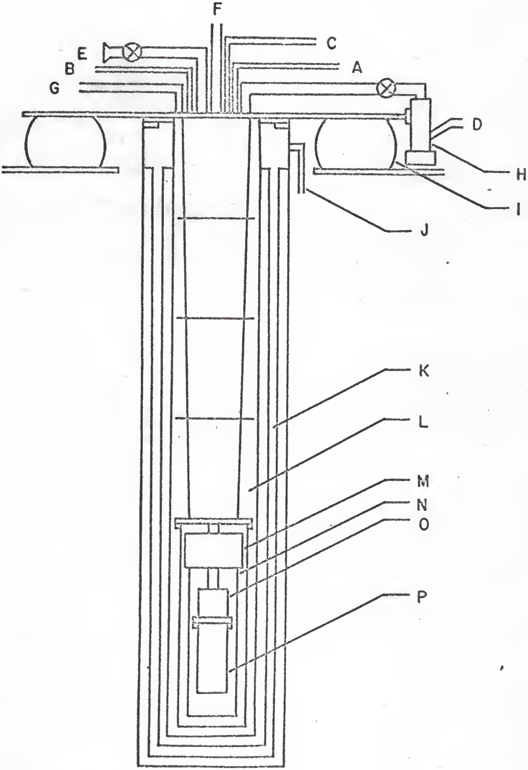
F
C
E
B
A
G
D
H
I
J
K
L
M
N
O
P

to the underside of the He^4 evaporator surrounds the He^3 evaporator and the sample chamber.

The He^3 refrigeration system was designed for continuous operation. The evaporator holds approximately 1 cm^3 of liquid He^3. A National Research Corporation model B-2 oil diffusion pump backed by a Welch model 1402 pump with an oil shaft seal for closed system operation can reduce the evaporator and the sample chamber temperature to nearly 0.3 K. The return gas is forced to pass through a trap immersed in liquid nitrogen. This trap consists of a stack of discs cut from brass screen followed by a container of Linde 13X molecular sieve pellets. The return line is constricted as it passes by the He^4 evaporator. This constriction, made by feeding a 10 mil nichrome wire through about 10 cm of 12-mil-i.d. stainless steel capillary, reduces the pressure of the returning He^3 which has been liquified in the constriction through thermal contact with the He^4 evaporator.

The sample chamber is bolted directly to the bottom of the He^3 evaporator, the abutting faces being lightly greased to improve thermal conduction. A copper vacuum-tight container encloses the sample chamber. The vacuum seal is again made using a gasket of pure indium wire. The sample chamber may be evacuated through a 0.127-cm-o.d. stainless steel capillary. If all systems perform properly at 4 K, He^3 exchange gas is introduced into the sample chamber.

Length changes of the sample are measured using a capacitance technique discussed later. The two capacitor leads and the two leads from a germanium resistance thermometer are coaxially shielded. There is a spare coaxially shielded lead. Such a line is constructed by passing a stainless steel capillary inside a 0.6-cm-diameter stainless steel tube extending from above the top cryostat flange to the vacuum seal flange

above the He^4 evaporator. Nylon spacers center the inner capillary which extends through a small glass-to-metal seal mounted in the bottom end of the tube. The capillary terminates a few inches below the top end of the tube. A length of copper wire soldered to the capillary is bent in a tight spiral before extending through another seal mounted in the upper end of the tube.

Eighteen leads made of formvar-insulated #34 Midohm wire enter the vacuum chamber through the vacuum chamber pumping line. The leads terminate at the top in two vacuum-tight nine-pin male connectors. All leads are thermally grounded to the vacuum seal flange and the He^4 evaporator. Only five of these leads are used and are thermally grounded to the He^3 evaporator: four leads serve two heater resistors and one lead is connected to a nominally 470-ohm Speer carbon resistor used as an uncalibrated thermometer during cool-down.

The reduction of vibration is crucial to the success of the experiment. The boiling of liquid nitrogen in the outer dewar (about 9 l.) is pumped continuously with a Kinney model KC-46 vacuum pump so the nitrogen is completely solidified. The pump is capable of 40 cfm, although our plumbing arrangements for pumping on the dewar are awkward and reduce this figure. Nevertheless, the nitrogen can be pumped below the triple point in about an hour.

The cryostat is supported entirely by a partly inflated automobile inner tube. Considerable vibration can be transmitted by the vacuum connections, however, unless special precautions are taken. Vacuum connection to the He^4 evaporator is made through a four-foot-long surgical rubber hose with a 3/4-inch-i.d. A weight suspended from the ceiling is clamped to the hose near its midpoint. The pumping line for the vacuum chamber needs to be quite large. After this chamber has been evacuated, a

valve at the top of the cryostat is closed and a quick-disconnect coupling in the vacuum line broken. The connections for the sample chamber capillary, the vapor pressure volume, and the He^3 gas return line are made via two-foot-lengths of 3/8-inch-i.d. stainless steel flexible tubing. The He^3 diffusion pump is attached near the top of the cryostat and is supported by the inner tube. A four-foot-long section of 1-inch-i.d. stainless steel flexible tubing connects the pump to a flange bolted to the wall. Another three-foot-long flexible tube connects this flange with the backing pump. A weight suspended by a wire from the ceiling is clamped to the tube near its midpoint. As this pump vibrates badly, the return line communicates with the plumbing on the cryostat support frame via a length of 3/8-inch-diameter stainless steel flexible tubing which also connects to a flange bolted to the wall.

Temperature Measurement and Control

Temperatures were measured and regulated by means of a germanium resistance thermometer used with the three-terminal ac bridge shown in Figure 3. The "three-terminal" designation is appropriate in that neither lead of the thermometer is grounded, and ground is used as a guard point. Resistances to ground do not greatly shift the null point but reduce the sensitivity to unbalance. This arrangement is analogous to the three-terminal capacitance bridge described elsewhere. Resistance of the leads is included, so recalibration is required after any change in the wiring which could change the lead resistance. The thermometer must be calibrated *in situ*.

We have used a General Radio model 1493 ratio transformer (seven decades plus slidewire) driven by the 400 Hz oscillator of the phase-sensitive detector, isolated by a Gertsch ST-100B shielded transformer. The

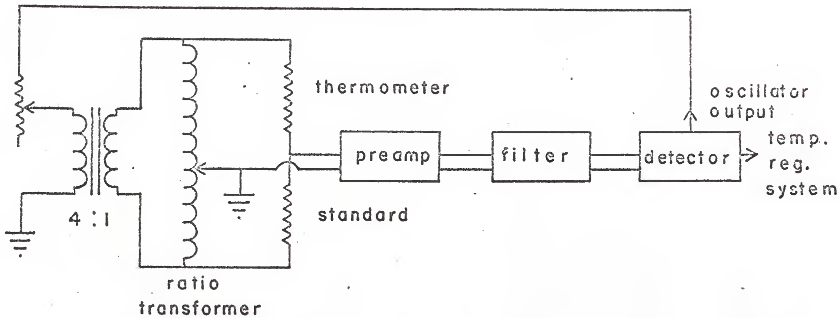

Figure 3. Simplified Schematic of the Resistance Bridge

unbalance is amplified by a Princeton Applied Research model Cr-4 preamplifier in the "low-Z double-ended" mode. A five-stage RC filter precedes final amplification with a Princeton Applied Research model 120 phase-sensitive detector.

The standard resistor is a 2 kilohm wirewound resistor sealed in a copper tube with epoxy and clamped in a heavy aluminum block for thermal ballast. Electrical connections are made via foot-long lengths of shielded leads constructed by passing thin stainless steel capillary through stainless steel tubes. This arrangement was designed to reduce the heat leak to the resistor. The entire assembly is encased in Styrofoam for further thermal shielding. No drifting of the resistance has ever been observed.

No provision is made for balancing the out-of-phase component. A variable capacitor placed across the thermometer leads has been found to work satisfactorily, but the additional sensitivity this affords is not necessary for the present experiment where the limiting factor is the vibration-induced capacitance fluctuations.

The potential across the standard resistor and thermometer in series is 0.1 volts, so at 1 K the power dissipated in the thermometer is about 0.4 μ W and decreases as the temperature decreases. The power dissipated at 4 K is approximately 40 μ W. Doubling the bridge voltage does not cause heating.

The detector output drives a single-stage common-base amplifier which controls the current through a heater resistor. This resistor is of the deposited film variety so its resistance is not strongly temperature-dependent. As the thermometer temperature drops, the heater current is increased so the sample chamber is warmed, and vice versa. An adjustment

of the sensitivity of the heater current, I, to detector output, V, is provided so that

$$I = \begin{cases} xV + \underline{I} & xV + \underline{I} > 0 \\ 0 & \text{otherwise} \end{cases}$$

where x is the fraction of the detector signal sent to the amplifier and $\underline{I}$ is a constant background current. The parameters x and $\underline{I}$ are easily adjusted.

The response is not instantaneous as temperature is not transmitted in copper with an infinite velocity. Therefore, if x is too large, the regulation becomes unstable and the temperature oscillates. For the same reason, it is difficult to use the regulator if the heater is too distant from the sensor. On the other hand, temperature gradients may exist across the sample chamber if the heater is adjacent to the thermometer. The regulator output may be switched between two resistors. One is located at the bottom of the sample chamber near the thermometer (refer to Figure 7). The other is mounted on the side of the He^3 evaporator. The more distant heater was used in all measurements in the critical region, although no temperature drifts were observed under any conditions when the heater nearer the sensor was used.

We were able to measure and regulate temperature to within 10 μ K, although our determination of the absolute temperature was not this accurate.

Temperature calibration is achieved by means of He^3 and He^4 vapor-pressure measurements. Liquid is condensed in a copper container with a volume of approximately 1 cc which is attached to the He^3 evaporator. To reduce the quantity of gas used, small (0.16-cm- and 0.32-cm-diameter) tubing was used for the lower sections of the vapor pressure line. At very low temperatures where thermomolecular correction is important, the

level of the liquid He^4 bath must be high enough to cover the junction to 0.62 cm tubing, as the temperature of this junction must be known. To reduce the possibility of non-equilibrium between the thermometer resistor and the liquid, no electrical heating is used during calibration runs. Readings are taken at approximately 50 mK intervals except at the lowest temperatures where the interval is decreased.

The He^4 calibration extends from the lambda point to 4.2 K. The 1958 He^4 vapor pressure scale is used. A 0.4% correction to our mercury manometer pressure readings must be applied to give the equivalent 0 C pressures. No calibration data are taken below the lambda point of He^4.

The He^3 calibration extends from below 0.4 K to just above the lambda point in liquid He^4. A Texas Instruments model 145 Precision Pressure Gauge with a type 1 Bourdon capsule designed for pressures from 0 to 300 Torr is used. The quartz tube in this capsule shows hysteresis effects so that even when the zero is readjusted immediately before the lowest pressure measurements, accuracy may not be better than a few microns. Pressures are corrected for the thermomolecular effect using the tables of Roberts and Sydoriak[56] for a 0.318-cm-radius tube extending from the helium bath to room temperature. This correction is negligible above 0.6 K. The T_{62} He^3 temperature scale is used to convert vapor pressures to temperature.

The temperature scale near 0.9 K where the transition occurs is not a closed subject. Clearly, small errors in the vapor pressure scale could lead to large errors in the expansion coefficient where the slope of the calibration curve is important. Such errors are not likely as the equation[57] from which the T_{62} scale is generated is semiempirical in that the temperature dependence is predicted theoretically and the data is used only to find coefficients. Slowly varying errors displace the critical temperature but do not change the shape of the expansion coefficient curve significantly.

As small resistance increments must be measured to determine precisely the shape of the capacitance-versus-temperature curve, a procedure to find the temperature as a smooth function of resistance is required. This function must satisfy two criteria. First, we cannot permit fluctuations in the temperature-versus-resistance curve such as might cause an irregular slope in the capacitance-versus-temperature curve. Second, the function must agree with the calibration points.

It is observed that the resistance, R, is a function of the temperature, T, obtained from the vapor pressure measurements of the form

$$T \simeq R^{-.518}$$

with only slight curvature. We thus attempt a machine fit of the form

$$T = \sum_{i=1}^{N} A_i \left(R^{-.518} \right)^{i-1} .$$

This form with N = 5 fits the temperature with an RMS deviation less than 1 mK above 0.6 K. The scatter in the vapor pressure measurements is greater than this at the lowest temperatures. Since there are but five smoothly varying terms, we expect that the calculated temperature will be a smooth function of the resistance. In practice, the program must initially calculate the resistance from the ratio transformer reading, X, using the relation

$$R = 2\text{K ohm} \times (1 - X)/X.$$

The large number of manipulations involved allows round-off error to deteriorate the quality of the fit. The program, diagrammed in Figure 4, therefore calculates corrections to the parameters A_i. The result of this program is a relation for the temperature as a function of the ratio transformer reading which satisfied our two criteria.

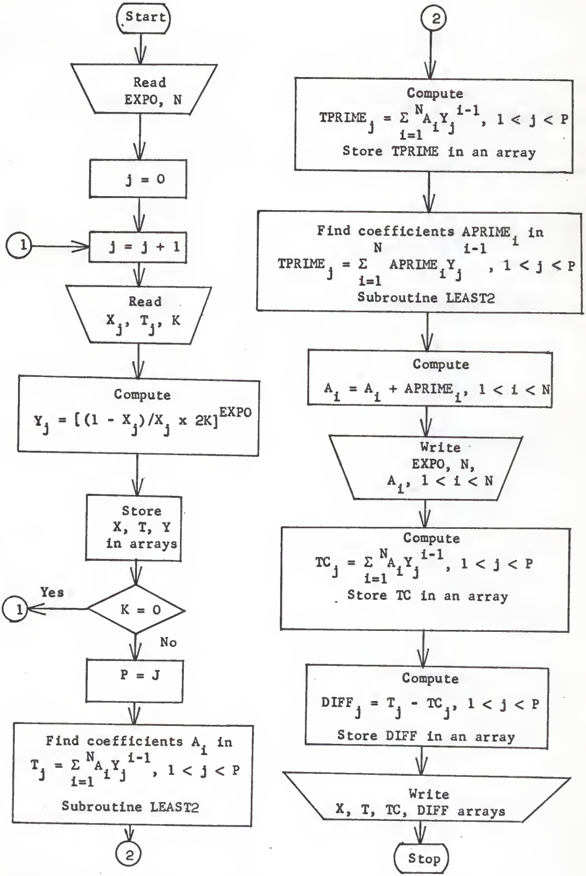

Figure 4. Flowchart of the Thermometer-Resistor Fitting Program

Measurement of Small Length Changes

Although the thermal expansion anomaly at the Curie temperature is quite large, the expansion coefficient changes rapidly with temperature, so in order to define the shape of the curve carefully, one must measure the length change over a small temperature interval. These resulting length changes are quite small. For example, our measurements for $CuK_2Cl_4 \cdot 2H_2O$ indicate that when the reduced temperature is 10^{-3} and the reduced temperature interval is $2x10^{-4}$, the relative length change $\Delta\, l_s/l_s \simeq 10^{-9}$. Furthermore, the available sample may be small so the length change is less than 0.1 Å. Recent reviews by Collins and White[58] and Swenson[59] indicate the sensitivities of various techniques employed to measure dilitation at reduced temperatures. In approximate order of increasing sensitivity these methods are the following:[58]

1. X-ray diffraction determines the lattice parameters as a function of temperature. A relative length resolution, $\Delta\, l_s/l_s$, of approximately $4x10^{-6}$ is obtained.

2. The two-terminal capacitance technique has been used to give a length resolution of 10^{-6}cm.

3. The optical interferometer resolves a length change of about 10^{-7}cm.

These methods are not sufficiently sensitive for our needs. Three techniques are capable of sufficient resolution:[59]

1. The differential motion of two grids,[60] one of which is coupled to the sample by means of a lever arrangement to increase the sensitivity, is sensed by two photocells. Sensitivity on the order of 0.1Å has been achieved.

2. The variable differential transformer[61] has been used with a

resolution up to 0.03 Å under special conditions. This is perhaps the most sensitive method available for thermal expansion measurement. Unfortunately, it is quite difficult to operate and is limited to liquid helium temperatures where the coil resistance is low and the geometry does not change.

3. The capacitance technique has been used to measure $\left(\frac{\partial P}{\partial T}\right)$ and the equation of state[62,63] as well as the thermal expansion coefficient as pioneered by White.[64] The technique has also been used near room temperatures.[38] A resolution of less than 0.1 Å is possible.

Capacitance Technique

Thompson[65] suggested the use of a "capacitance probe" which would consist of a guard ring and a disk parallel to another surface. Sample chambers suitable for low-temperature differential or absolute thermal expansion measurements are described by White.[64]

It is necessary to find the relation between the capacitance and the thermal expansion coefficient of the sample for a typical geometry such as that shown schematically in Figure 5. It is convenient to divide the problem into three parts. First, we find the relation between the thermal expansion coefficient of the sample and the temperature derivative of the plate separation. Next, we assume parallel plates to find α in terms of the reciprocal of the capacitance. Finally, we consider in an approximate fashion the effect of nonparallel plates.

To undertake the first part of the problem, assume the plate and crystal supports, the sample chamber frame, and the capacitor plates are all constructed of copper having a thermal expansion coefficient given exactly by α_{Cu}. Referring to Figure 5, it is clear we need only consider the expansion of copper over a length l_c equal to the sample length, l_s, plus the plate separation, g. Therefore, we have

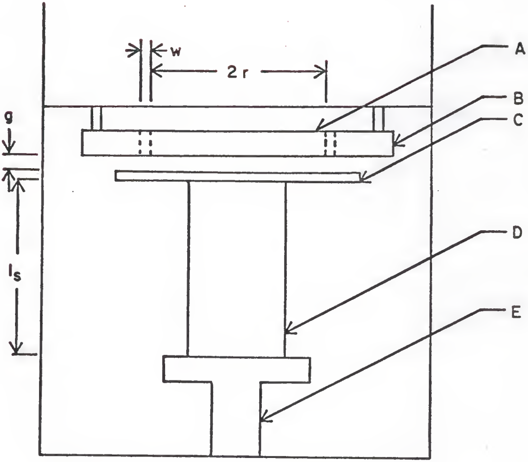

Figure 5. Simplified Drawing of the Sample Chamber

A. Guarded (fixed) plate
B. Guard ring
C. Moveable plate
D. Sample
E. Sample support

$$l_c = l_s + g.$$

Upon taking the temperature derivative, we have

$$\frac{dl_c}{dT} = \frac{dl_s}{dT} + \frac{dg}{dT} = l_s\,(1 + g/l_s)\,\alpha_{Cu}$$

or

$$\alpha = \frac{1}{l_s}\,\frac{dl_s}{dT} = (1 + g/l_s)\,\alpha_{Cu} - \frac{1}{l_s}\,\frac{dg}{dT}\,. \qquad [1]$$

We will find that the neat cancellation of thermal expansion of construction materials over comparatively great lengths is probably not valid.

Next, the relation of $\frac{dg}{dT}$ to the capacitance and its derivative must be determined. Referring again to Figure 5, note that the guarded plate has radius r and the guard ring gap is of width w. The other plate is assumed parallel and at a distance g. The capacitance, C, between the plates is given by Maxwell[66] as follows:

$$C = \frac{\epsilon_o \pi r^2}{g}\left[1 + \frac{w(1 + w/2r)/r}{1 + 0.22w/g}\right]. \qquad [2]$$

Define l_{eq} by

$$C = \frac{\epsilon_o \pi r^2}{l_{eq}}$$

and let

$$a = \frac{w}{r}\left(1 + \frac{w}{2r}\right)$$

and $b = 0.22w$.

Now Eq. [2] becomes

$$l_{eq}^{-1} = g^{-1}\,[1 + a(1 + b/g)^{-1}],$$

or

$$2g = (a + 1)l_{eq} - b + \{[(a + 1)l_{eq} - b]^2 + 4bl_{eq}\}^{1/2}. \qquad [3]$$

We assume the guard ring and the plates have the same expansion coefficient. Then we find

$$\frac{d}{dT}\left(\frac{w}{r}\right) = \frac{d}{dT}\,[(w + r)/r - 1] = 0.$$

It therefore follows that

$$\frac{da}{dT} \doteq 0.$$

The derivative $\frac{dg}{dT}$ is found directly from Eq. [3]. For our expansion chamber, the values of w and r are given by

$w = 0.051$ mm

and $r = 0.70$ cm,

so that $a = 4\times10^{-3}$. Before writing down the expression for $\frac{dg}{dT}$, we make the approximation

$$a + 1 \simeq 1$$

and $g/l_{eq} = 1 + a/(1 + b/g) \simeq 1.$

Then we have

$$\frac{dg}{dT} = \frac{dl_{eq}}{dT} + 1/2\,[(1 + b/l_{eq})/(1 - b/l_{eq}) - 1]\,\frac{db}{dT}, \qquad [4]$$

with

$$\frac{dl_{eq}}{dT} = 2l_{eq}\alpha_{Cu} + \epsilon_o\,\Pi r^2\,\frac{dC^{-1}}{dT}. \qquad [5]$$

During the experiment described here,

$$C = 20.6 \text{ pf}$$

and $$l_s = 0.38 \text{ cm.}$$

Therefore, we have

$$b/l_{eq} = 0.17$$

and $$l_{eq} = 0.0065 \text{ cm.}$$

Substituted into Eqs. [4] and [5], this gives

$$\frac{1}{l_s}\frac{dg}{dT} = \frac{1}{l_s}\frac{dl_{eq}}{dT} + 6\text{x}10^{-4}\,\alpha_{Cu}$$

with

$$\frac{1}{l_s}\frac{dl_{eq}}{dT} = 0.34\,\alpha_{Cu} + 0.36 \text{ pf}\,\frac{dC^{-1}}{dT}.$$

Finally, substituting these results into Eq. [1], we have

$$\begin{aligned}\alpha &= 1.017\,\alpha_{Cu} - \frac{1}{l_s}\frac{dg}{dT} \\ &= 1.017\,\alpha_{Cu} - [(0.034\,\alpha_{Cu} + 0.36 \text{ pf}\,\frac{dC^{-1}}{dT}) + 6\text{x}10^{-4}\,\alpha_{Cu}] \\ &= 0.98\,\alpha_{Cu} - 0.36 \text{ pf}\,\frac{dC^{-1}}{dT}.\end{aligned} \qquad [6]$$

Now we come to the final part of the problem, the effect of non-parallel plates on $\frac{dg}{dT}$. For the purpose of this discussion neglect fringing effects so the infinite parallel plate capacitor formula can be used. Suppose the upper plate is tilted about the y-axis. The x-axis is assumed to lie in the plane of this plate with the origin of the coordinate system at the center of the plate. Then consider the area $2(r^2 - x^2)^{1/2}dx$ at a distance $(g + x \sin \theta)$ from the lower plate, where θ is the angle between the plates and g is the separation of the centers. The projection, dA, of this area on a plane parallel to the lower plate is

$$dA = 2(r^2 - x^2)^{1/2} \cos\theta \, dx.$$

The capacitance in the present approximation is given by

$$C = \epsilon_o \int_{-r}^{+r} [2(r^2 - x^2)^{1/2} \cos\theta]/(g + \sin\theta) \, dx$$

$$= 2\Pi \epsilon_o \cot\theta \{\frac{g}{\sin\theta} - [(g/\sin\theta)^2 - r^2]^{1/2} \},$$

or

$$g = \frac{C \sin^2\theta}{4\Pi \epsilon_o \cos\theta} + \frac{\Pi r^2 \epsilon_o \cos\theta}{C} .$$

Hence, we have

$$\frac{1}{l_s}\frac{dg}{dT} = (1 - \phi^2) \cos\theta \; \frac{\Pi r^2 \epsilon_o}{l_s} \quad \frac{dC^{-1}}{dT} \qquad [7]$$

where

$$\phi = \frac{C \tan\theta}{2\Pi r \epsilon_o} .$$

If we define l_{eq} as before, and let

$$\Delta = 2r \sin\theta,$$

then $\phi = \frac{1}{4}\frac{\Delta}{l_{eq}}$.

We cannot evaluate the angle θ, but since it is not expected to change for the small length changes observed below 4 K, and since l_{eq} (or C) is approximately constant in this temperature range, we may consider that the factor $(1 - \phi^2) \cos\theta$ in Eq. [7] introduces a small but constant uncertainty in the determination of the expansion coefficient. It does not affect the <u>shape</u> of the expansion curve, however.

To estimate an order-of-magnitude value for the correction, assume that the plates are set at room temperature with an error Δ/g less than $1/4$, and that ϕ does not increase greatly as the temperature is reduced. Then the constant error introduced into the determination of the linear expansion coefficient is less than 1% when $C \doteq 20.6$ pf.

It is possible to measure the angle θ if the guarded plate is replaced by two concentric plates. At room temperature with the plates parallel, the area ratio is determined from the ratio of the capacitance of the inner plate with the outer one grounded to the capacitance of the outer plate with the inner one grounded. The guard ring is always grounded. Then at low temperature, the angle can be calculated from the ratio of the capacitances. Such an arrangement was used in the present sample chamber, but imaginary angles were indicated ocassionally. It is probable that the method used to construct the plates allowed the inner plate to drop slightly with respect to the other upon cooling.

Two methods are generally used to measure small capacitances. The capacitor may be made a part of a resonant circuit so length changes are measured as frequency changes.[63] We have used an alternate method which involves direct measurement of the three-terminal capacitance by means of a bridge circuit. One uses a three-terminal technique so that stray capacitances between the plates and the leads to ground shunt the detector but do not greatly change the null point. The variable component of the bridge may be the transformer and/or the capacitance. We have used the General Radio Type 1615-A capacitance bridge complemented by a 1404-B 100pf standard capacitor and driven by a General Radio 1311-A audio oscillator operated at 5 KHz and 10 volts. The General Radio 1232-A tuned amplifier and null detector is used in the untuned mode as a preamplifier for a Princeton Applied Research HR-8 phase sensitive detector. The bridge employs a ratio

transformer tapped at intervals of one-tenth, and eight standard capacitors, six of which are used at once. A simplified diagram of the bridge is shown in Figure 6.

One deficiency of this system is its dependence on ambient temperature. The external standard has a temperature coefficient of 2×10^{-4} pf/C, while the stability of the bridge is limited by the temperature coefficient of the 10 pf standard which is less than 5×10^{-5} pf/C. The external standard is therefore housed in a Styrofoam-packed container. The bridge itself cannot be well isolated since controls must be accessible, and levers or shafts constitute a heat leak which is difficult to reduce. The bridge is therefore enclosed in a Styrofoam box with extensions on the balance levers extending through slots cut in a heavy-gauge aluminum front panel. The temperature of another aluminum plate inside the box and beneath the bridge is regulated by the amplified out-of-balance signal from a bridge circuit with a thermistor in one arm. Although the temperature of the room was coarsely regulated, a small drift of the measured capacitance was sometimes observed which could be correlated with room temperature changes. Such drifts were not of sufficient magnitude to change the shape of the measured expansion coefficient, however.

The expansion chamber used in the measurements reported here is shown in Figure 7. The sample bears directly on the under side of a flat disc which serves as one of the capacitor plates. This plate is held under tension against the sample by a thin brass bellows which exerts a small vertical force. The bellows ends below the sample so the platform upon which the sample rests is larger than the inner diameter of the bellows (approximately 1.1 cm). Since the platform and the sample is not limited in size by the bellows, wide samples may be used. Wide samples are desired since the support for the capacitor plate must be as steady as possible. Three

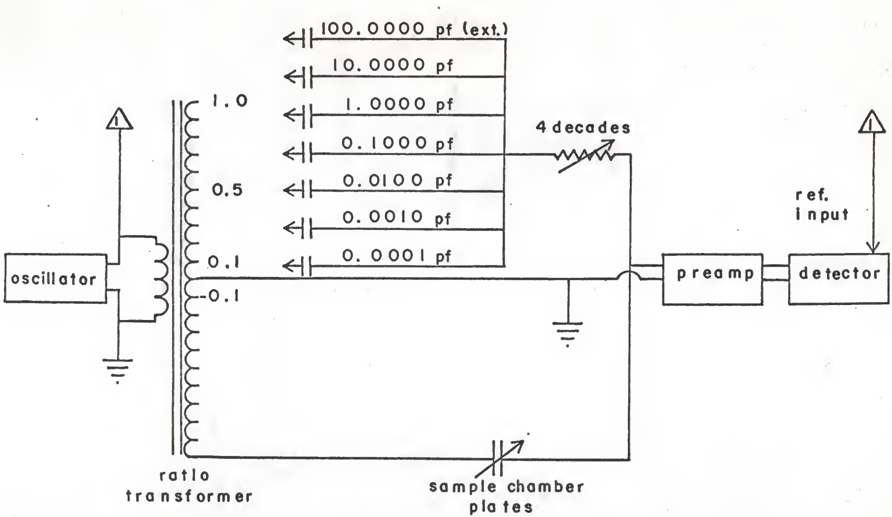

Figure 6. Simplified Schematic of the Capacitance Bridge

Figure 7. The Sample Chamber

A. Flange for indium gasket

B. Vacuum-tight electrical connector

C. Differential screw for fine adjustment of plate separation

D. Screw for coarse adjustment of plate separation

E. Spring

F. Guarded (stationary) capacitor plate

G. Guard ring

H. Moveable capacitor plate

I. Sample

J. Nylon post

K. Thin-walled brass bellows

L. Heater resistor

M. Germanium resistance thermometer

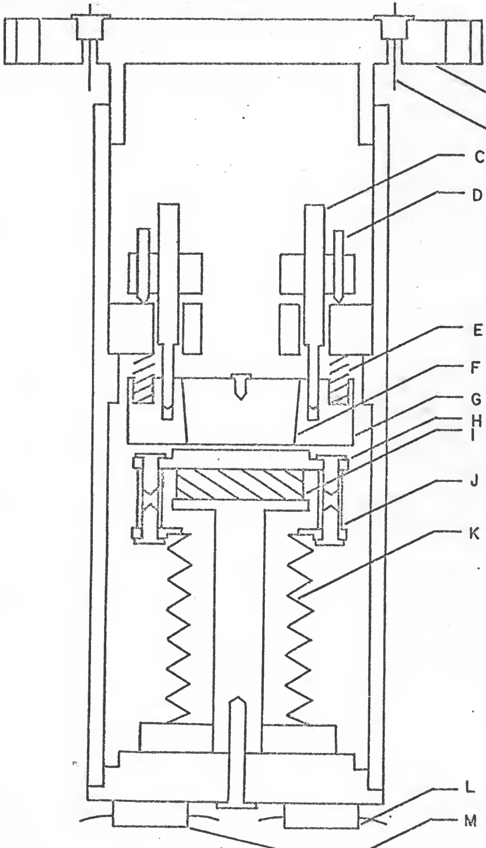
A
B
C
D
E
F
G
H
I
J
K
L
M

posts connect the bellows to the plate. The spaces between the posts permit easy access to the platform upon which the sample rests so that it is easy to determine that the sample is properly positioned. The posts are made of nylon since the lower plate must be electrically insulated from the sample chamber. The bellows and nylon posts serve to maintain tension on the upper plate but they do not affect the plate spacing.

The method of constructing the plate-guard ring assembly was suggested by Dr. C. A. Swenson and is due to Dr. G. K. White. The plate is machined as a plug with a taper of about 1%. Two layers of 1 mil mylar are wrapped around the plate before it is tapped into a mating hole in the guard ring. Finally, both flat sides are machined smooth, considerable care being required to avoid leaving copper in the gap. One can check that the plate will remain secure at low temperatures by immersing the assembly in liquid nitrogen.

The height and angle of this plate may be adjusted over a wide range to facilitate installation of samples with slightly varying sizes and shapes. Provision is also made for setting the plate with a "negative gap" at room temperature so that a sample with an expansion coefficient much larger than that of copper can still be used with a small gap at 4 K, as required for high sensitivity. The mechanism supporting the plate is shown in Figure 6. Three screws support a brass ring from the sample chamber frame. These screws provide a coarse adjustment of the plate position. Three differential screws support the plate-guard ring assembly below the ring. The motion of the 4-48 section in the brass ring is partly cancelled by the motion of the 2-56 section in the guard ring so the net displacement is equivalent to a screw with 336 threads per inch, but our arrangement is much stronger. Three springs push down on the guard ring so the coarse adjusting screws are held firmly against the expansion chamber frame. Motion due to

play in the threads is reduced by lightly greasing the screws so that at low temperatures, where the grease solidifies, the threads are held tightly.

The plates are adjusted by trial-and-error procedures. With the sample in place, the coarse adjusting screws are used to bring the upper plate close to the lower one. Then the differential screws are rotated until the desired capacitance is reached and the plates appear to be parallel. A strong light behind the plates facilitates this adjustment. We have observed that the net contraction of the $CuK_2Cl_4 \cdot 2H_2O$ sample is similar to that of copper, so the plate setting does not change greatly between room and liquid helium temperatures. This has not been true with other materials we have studied, so several room temperature gaps must be tried before a suitable 4 K gap is attained.

Eq. [6] indicates that the measured expansion is given by 0.36 pf/C^2 ΔC for small capacitance changes. The bridge detects a ΔC of 10^{-6} pf provided one figure can be interpolated on the HR-8 detector. This gives a length resolution, $\Delta l_s/l_s$, of 8.5×10^{-10} when the capacitance is 20.6 pf. Vibration of the plates caused fluctuations of two or three in the interpolated figure so the resolution was reduced to about 3×10^{-9}. This corresponds to a length change of approximately 0.1 Å for our small (0.38 cm) sample.

CHAPTER IV

EXPERIMENTAL RESULTS AND DISCUSSION

Analysis of the Data

This chapter describes how the capacitance-versus-resistance data are analyzed to give the linear expansion coefficient, $\alpha = \frac{1}{l_s} \frac{dl_s}{dT}$, in the a direction of a single crystal of $CuK_2Cl_4 \cdot 2H_2O$ from 0.4 K to 4.2 K. Particular attention is given to the data in the critical region near T_c and in the high-temperature region above 2 T_c. From data in these two regions, information is obtained about the stress dependence of the exchange parameters and the behavior of the spin correlation functions discussed in Chapter II. In addition, the stress derivative of the transition temperature is determined.

The raw data consist of approximately 600 capacitance values versus resistance-bridge ratio-transformer settings. Two sets of data cover the range from 0.35 K to 4.2 K. Several data sets were taken in the critical region both warming and cooling. As each pass defines the transition point more precisely, the next pass covers a smaller temperature range with a greater point density. The temperature interval on the final set is approximately 100 μK, giving a capacitance interval of about 10^{-6} pf, the limit of our resolution.

The first step in the analysis is the same for all data points. The

temperature for each point is machine calculated as described in the previous chapter. As we have seen, the derivative of the inverse of the capacitance is required (Eq. [6] of Chapter III). Hence it was decided to work with the inverse of the capacitance from the outset. The computer program is designed to convert the raw data to reciprocal capacitance-versus-temperature points. This information is punched on cards and printed for further analysis.

Physical shocks of the expansion chamber cause the capacitance to shift discontinuously. Such shifts sometimes occur when valves on the cryostat support frame are turned, when heavy objects are dropped on the laboratory floor, and when liquid nitrogen or liquid helium is transferred. In addition, the standards in the capacitance bridge drift slowly. It is therefore necessary to shift the inverse capacitance of each data set by a constant to bring the curves into coincidence. These constants correspond to shifts of less than 0.1% in the capacitance for data taken over a period of five days. Further analysis is based on the shifted reciprocal capacitance-versus-temperature data. A few of these points are shown in Figure 8.

At temperatures greater than 1.5 K, the thermal expansion coefficient is expected to vary as T^{-2}. As the expansion is quite small in this temperature range, the thermal expansion of the chamber cannot be neglected. Hence the measured expansion given by Eq. [6] of Chapter III is expected to obey a relation of the form

$$\alpha - 0.98\,\alpha_{Cu} = -0.36\ \mathrm{pf}\ \frac{dC^{-1}}{dT}$$

$$= aT^{-2} + bT + cT^{3},$$

where the T and T^3 terms are included for the electronic and lattice con-

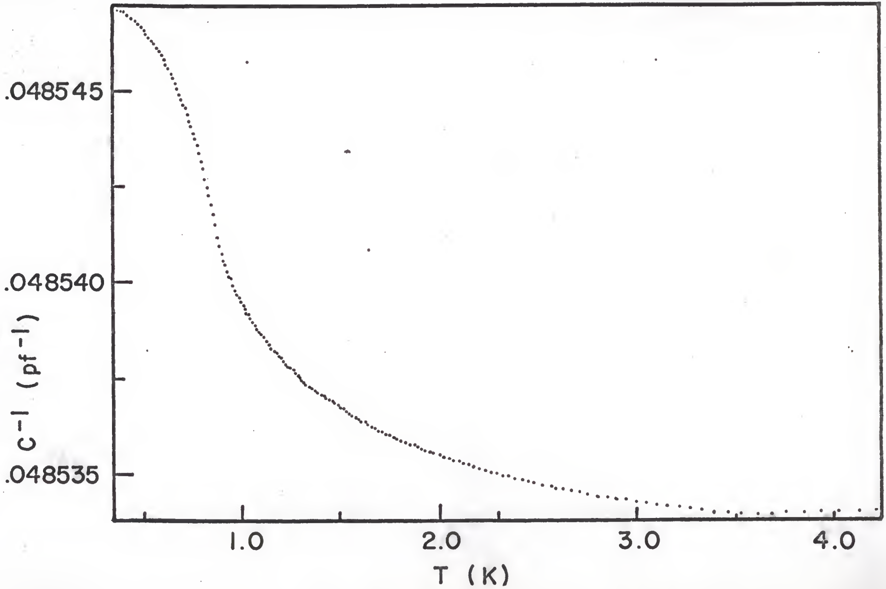

Figure 8. The Reciprocal of the Capacitance vs Temperature

tributions, respectively, of copper. We integrate the form predicted for the expansion coefficient to find a form for the reciprocal capacitance. The coefficients in the resulting equation are found by a least-squares fit to the data. When the fitted equation is differentiated, the result is

$$10^8(\alpha - 0.98\,\alpha_{Cu}) = 2.16T - 0.508T^3 + 289T^{-2}.$$

Carr and Swenson[67] have found that in this temperature range,

$$10^8\,\alpha_{Cu} = 1.7\times10^{-2}T + 10^{-3}T^3.$$

This correction is much too small to account for the observed T and T^3 coefficients. The formula we have used is wrong for two reasons, however. First, the derivation of Eq. [1] of Chapter III required the cancellation of copper expansion over lengths greater than 5 cm. This copper is of commercial grade, not OFHC, and different parts were cut from stock purchased at different times. Second, the screws supporting the upper capacitor plate are made of brass with unknown expansion coefficient.

Although the total measured thermal expansion coefficient changes from $140\times10^{-8}K^{-1}$ to $10\times10^{-8}K^{-1}$ between 1.5 K and 4.1 K, this change is well described by the three-term fit which has the form expected for a T^{-2} magnetic contribution as well as an electronic contribution proportional to T and a lattice contribution proportional to T^3. While it is not possible to predict the sample chamber behavior, it is not unreasonable that the T and T^3 terms are sample chamber effects.

A fit from 1.5 K to 3 K gives nearly the same coefficient for the T^{-2} term, although the contribution from the T and T^3 terms at 3 K is only about 20% of the total measured expansion coefficient and decreases rapidly with temperature. At 2.5 K the contribution is less than the experimental error. Therefore, we find

$$\alpha \propto T^{-2} \quad 1.5\ K < T < 2.5\ K.$$

Such behavior is not inconsistent with the data to 4.2 K as discussed above. The results of the fit are summarized in Table 3.

At temperatures below 2.5 K, where the correction for sample chamber effects is negligible, Eq. [6] of Chapter III gives

$$\alpha = -\ 0.36\ \text{pf}\ \frac{dC^{-1}}{dT}\ .$$

In principle, one could take simple differences between points to find

$$\alpha\left(\frac{T + T'}{2}\right) = -\ 0.36\ \text{pf}\ \frac{(C')^{-1} - C^{-1}}{T' - T}\ .$$

The scatter in the data makes this procedure useless for closely spaced points.

Outside the critical region where the shape of the capacitance curve varies slowly, we use a local fit procedure which fits N consecutive data points to a linear form

$$C^{-1} = (C_o^{-1})_i + A_i T \qquad T_i < T < T_{i+N-1},$$

so that $\alpha_i(T_{av,i}) = -\ 0.36\ \text{pf} \times A_i.$

Values of N used range from four to twelve depending on the scatter and the density of points. The program prints the α_i and $T_{av,i}$ for any desired sequence of N's. Figure 9 shows the expansion coefficient versus temperature. Above 2.5 K, the fitted T^{-2} component is shown as a broken line.

This procedure is not valid quite near the transition, for the shape of the capacitance curve varies rapidly. If there is no scatter in the measurements, a straight line fit over a range of temperatures gives a

TABLE 3. Results of the Least-Squares Fits

<u>$T > 1.5$ K</u>

$$\alpha = (290 \pm 10)\times 10^{-8} K/T^{2}$$

<u>$10^{-2} < \epsilon < 10^{-1}$</u>

logarithmic law

$$\alpha = [-(470 \pm 30)\log\epsilon + 190^{a}]\times 10^{-8}K^{-1} \qquad T < T_c$$

$$\alpha = [-(470 \pm 30)\log\epsilon - 50^{a}]\times 10^{-8}K^{-1} \qquad T > T_c$$

power law

$$\alpha = [86.8^{b}\,\epsilon^{-1/(2.0 \pm 1.0)} + 406^{b}]\times 10^{-8}K^{-1} \qquad T < T_c$$

$$\alpha = [30.5^{b}\,\epsilon^{-1/(1.3 \pm 0.4)} + 230^{b}]\times 10^{-8}K^{-1} \qquad T > T_c$$

[a] Function of the coefficient of the logarithmic term. This value corresponds to the coefficient given.

[b] Function of the exponent. This value corresponds to the exponent given.

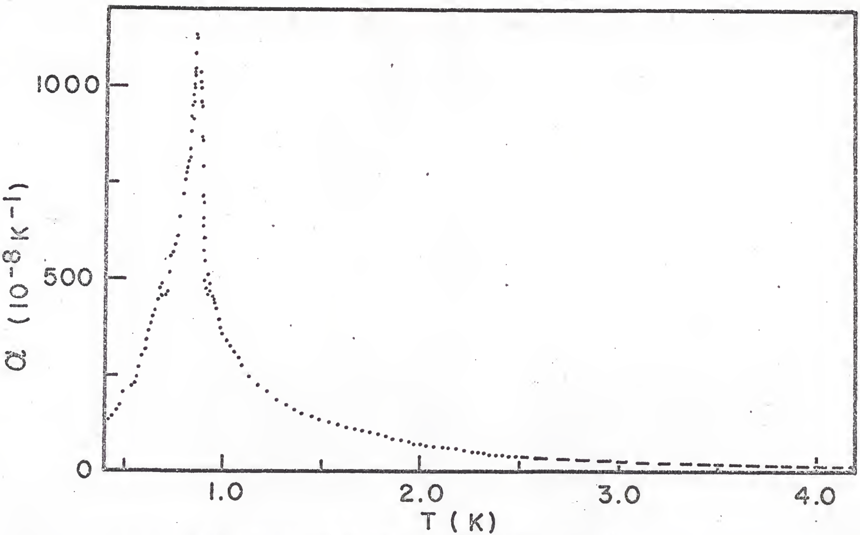

Figure 9. The Linear Expansion Coefficient vs Temperature

The T^{-2} dependence calculated from the fitted equation is shown above 2.5 K as a dashed line.

derivative similar to the quotient of differences $\frac{\Delta C^{-1}}{\Delta T}$ for a somewhat smaller range Δ T. Suppose the expansion coefficient follows a logarithmic law so that

$$C^{-1} = P + Q\,\epsilon + R \log \epsilon.$$

Then for $\Delta \epsilon \ll \epsilon_{av}$,

$$\frac{\Delta C^{-1}}{\Delta T} = \frac{d}{dT}(P + Q\,\epsilon)\Big|_{av} + \left(1 + \frac{\Delta \epsilon}{\epsilon}\right) \frac{d}{dT}(R \log \epsilon)\Big|_{av},$$

where average values are evaluated at the midpoint of the reduced temperature interval. The second term on the right dominates in the critical region, so that we have

$$\frac{\Delta C^{-1}}{\Delta T} = \left(1 + \frac{\Delta \epsilon}{\epsilon_{av}}\right) \frac{dC^{-1}}{dT}\Big|_{av} \quad \text{near } T_c.$$

For example, when $\epsilon_{av} = 10^{-2}$ and $\Delta \epsilon = 4 \times 10^{-3}$, the difference between $\frac{\Delta C^{-1}}{\Delta T}$ and $\frac{dC^{-1}}{dT}$ is 40 %. Clearly, another procedure must be found for use in the critical region.

Before proceeding with a machine fit, it is useful to estimate T_c. Suppose the expansion coefficient follows a logarithmic law so that

$$\alpha = A \log \epsilon + B.$$

Then we have

$$|T(\alpha + \Delta \alpha) - T_c| = 10^{\Delta\alpha/A} |T(\alpha) - T_c|.$$

A plot of $T(\alpha + \Delta \alpha)$ versus $T(\alpha)$ for some convenient $\Delta \alpha$ over the temperature range for which the logarithmic dependence holds is called a "Mangelsdorf retarded function plot."[68] The resulting straight line intersects

the line $T(\alpha + \Delta\alpha) = T(\alpha)$ at the Curie temperature. This plot determines the transition temperature and checks the logarithmic dependence. Unfortunately, this technique is only useful in the part of the critical region where the local fitting technique can be used to find the expansion coefficient, as smooth values for α are required. The plot shown in Figure 10 for $10^{-2} < \epsilon < 10^{-1}$ shows the failure of the logarithmic function for $T > T_c$, and predicts the transition temperature with an expected error of about $\pm$ 1.0 mK.

A simple perturbation procedure gives the critical behavior of the expansion coefficient. A form which exhibits approximately the observed temperature dependence is selected so the deviations will be small. The integral of this form is the equation to which the data are fitted. A considerable simplification to the fitting procedure is effected by treating T_c as a known parameter which is tried at various values in a small range about the temperature predicted by the Mangelsdorf plot. The output of the fit program consists of the value of $D = (C^{-1})_{fit} - (C^{-1})_{obs}$ versus reduced temperature for each point and the coefficients in the equation for the expansion coefficient. Then since

$$\alpha = -\,0.36\,pf\,\frac{d(C^{-1})_{obs}}{dT} = \alpha_{fit} + 0.36\ pf\,\frac{dD}{dT},$$

the correction to the fit may be calculated by taking the temperature derivative of the difference, D, which will be smoothly and slowly varying if the choice of function to be fitted is good. The derivative is found by taking slopes of a hand-smoothed plot of D versus T.

This procedure has been used for the form which fitted the specific heat,[20] i.e.,

$$\alpha_{\pm} = A \log \epsilon + B_{\pm}.$$

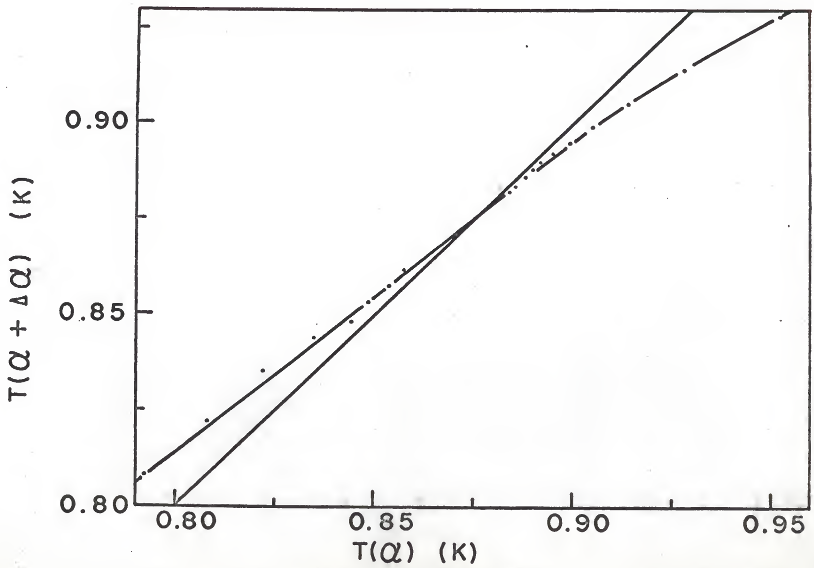

Figure 10. Mangelsdorf Plot for Reduced Temperatures in the Range 10^{-2} - 10^{-1}

The RMS deviation describing the capacitance fit is a function of the weighting factor applied to the points. Since the supercritical region is large, points more distant from the transition must be weighted more heavily. A good fit was found with a weight proportional to the reduced temperature. However, the fit is not a strong function of the exact nature of the weighting factor. The RMS deviation is not a strong function of the Curie temperature chosen as points quite near the transition are given little weight.

The result of the fit is given in Table 3 and is shown as the broken straight line on the semilog plot of Figure 11 for $T < T_c$ and Figure 12 for $T > T_c$. Points derived using the local fit are shown for $10^{-2} < \epsilon < 10^{-1}$. The continuous line shows the value of α near T_c calculated from the results of the fit as described above.

A fit to the form

$$\alpha_{\pm} = A_{\pm}\,\epsilon^{-1/n_{\pm}} + B_{\pm}$$

has also been made. The n's are treated as known parameters in the fit, and a wide range of values have been tried. As the power law gives a greater deviation in the supercritical region, this fit is a stronger function of the weighting factor than the logarithmic fit. Therefore, only points in the range $10^{-2} < \epsilon < 10^{-1}$ are considered, each with an equal weight. The RMS deviation is not a strong function of the critical temperature since points quite near the transition are not included in the fit. The expansion coefficient was not calculated near T_c as the deviations, D, are large and the results should be less accurate than values calculated from the logarithmic fit.

The results of the fit are given in Table 3 and are shown as the broken curve on the semilog plot of Figure 13 for $T < T_c$ and Figure 14 for

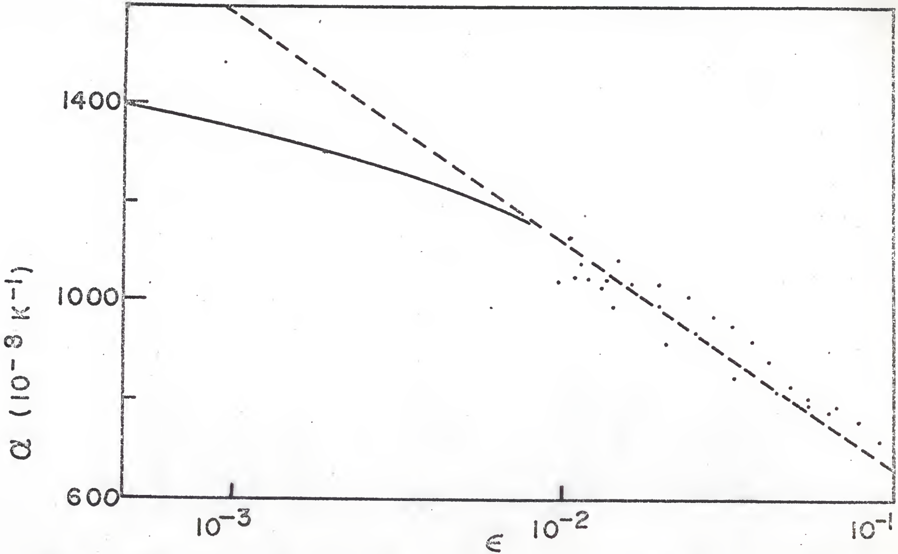

Figure 11. Semilog Plot of the Linear Expansion Coefficient in the Critical Region Below the Transition vs Reduced Temperature Showing the Results of the Logarithmic Law Fit.

The broken line gives the result of the logarithmic law fit. The smooth lines shows the expansion coefficient calculated from the results of the fit.

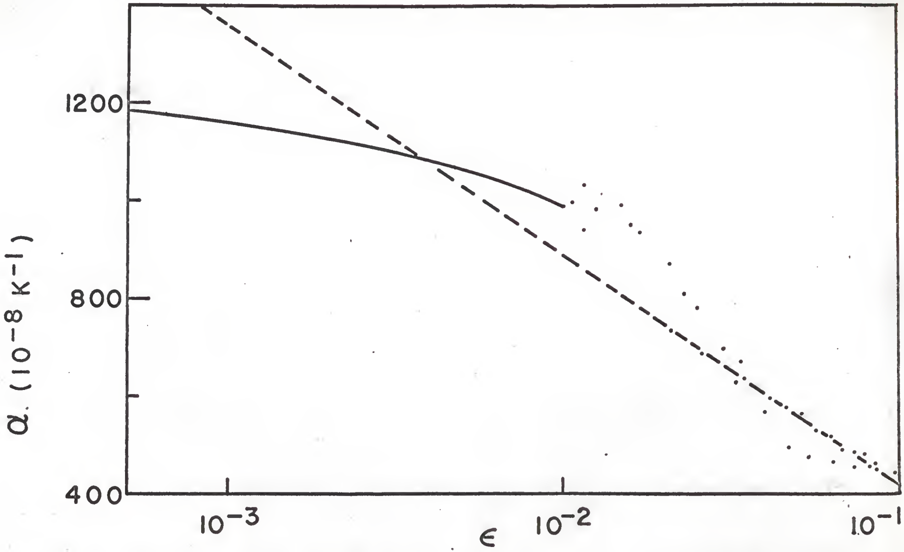

Figure 12. Semilog Plot of the Linear Expansion Coefficient in the Critical Region Above the Transition vs Reduced Temperature Showing the Results of the Logarithmic Law Fit

The smooth line shows the expansion coefficient calculated from the results of the fit. The broken line gives the result of the logarithmic law fit.

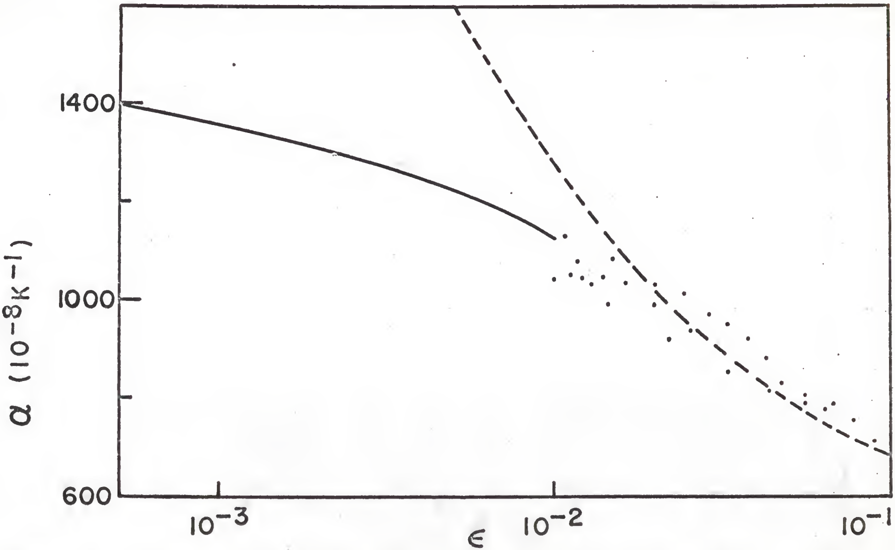

Figure 13. Semilog Plot of the Linear Expansion Coefficient in the Critical Region Below the Transition vs Reduced Temperature Showing the Results of the Power Law Fit

The broken line gives the result of the power law fit. The smooth line shows the expansion coefficient calculated from the results of the logarithmic law fit.

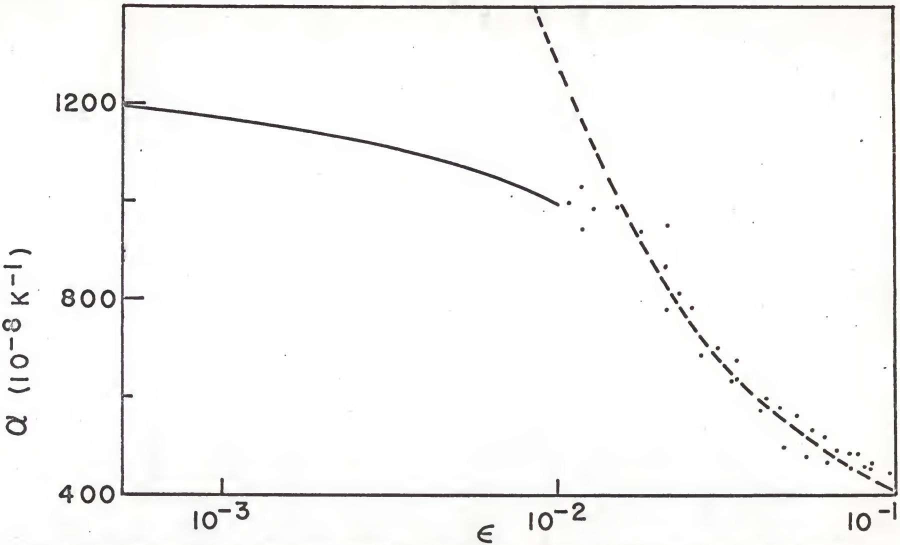

Figure 14. Semilog Plot of the Linear Expansion Coefficient in the Critical Region Above the Transition vs Reduced Temperature Showing the Results of the Power Law Fit

The smooth line shows the expansion coefficient calculated from the results of the logarithmic law fit. The broken line gives the result of the power law fit.

$T > T_c$. Points derived using the local fit are shown for $10^{-2} < \epsilon < 10^{-1}$. The smooth line is the value of α calculated from the logarithmic fit.

Comparison with the Specific Heat

A comparison of the results of the high-temperature fit given in Table 3 with the high-temperature specific heat results of Miedema, *et al.*,[20] leads to two conclusions.

1. For temperatures above 2 T_c, the nearest and next-nearest neighbor spin correlation functions have proportional temperature derivatives and/or the exchange constants have the same stress dependence. The analysis of the critical region results suggests the latter is false so that the spin correlation functions must have proportional temperature derivatives.

2. The Callen and Callen cluster expansion results[19] indicate the correlation functions have equal temperature derivatives so the shift of the Curie point with stress can be calculated using Eq.[5] of Chapter II. We find

$$\left(\frac{\partial T_c}{\partial \sigma_1}\right)_{\sigma_{j/1}} = -(1.40 \pm 0.09)\mathrm{x}10^{-11}\mathrm{K\ cm^2/dyne},$$

where the subscript 1 refers to the a direction.

Perhaps the most striking feature of our data is the severe rounding of the lambda peak. The supercritical region extends to a reduced temperature, ϵ_s, of almost 10^{-2}. The discussion of Chapter I led to a relation between ϵ_s and the number of magnetic ions, N, in a volume defined by the spin-fluctuation mean free path as follows:

$$N \sim \epsilon_s^{-3} \underline{\sim} 10^6.$$

This corresponds to a mean free path of about 500 Å extending over about 100 unit cells. The problem is to predict the asymptotic behavior of the expansion coefficient of a perfect sample from the available data which are limited to the reduced temperature range 10^{-2} - 10^{-1} where the spin coherence length is not on the order of the temperature-independent mean free path.

A log-log plot of specific heat versus reduced temperature (Figure 5 of Ref. 20) indicates that the behavior determined in the reduced temperature interval 10^{-2} - 10^{-1} differs from that determined in the range 10^{-3} - 10^{-2} if one assumes a power law. It is not correct to extrapolate the asymptotic behavior from observations in the more distant decade. This indicates that the power law is not appropriate over a wide temperature range. On the other hand, a semilog plot of specific heat versus reduced temperature (Figure 4 of Ref. 20) indicates the asymptotic behavior may be extrapolated from the reduced temperature interval 10^{-2} - 10^{-1} if a logarithmic form is assumed. The thermodynamics of Chapter II indicates the critical behavior of the thermal expansion coefficient should be linearly related to the specific heat, so these conclusions are expected to apply to the expansion coefficient also.

The Mangelsdorf plot (Figure 10) and comparison of the fitted expansion to the measured values (Figures 11 and 13) suggest the behavior in the critical region below the transition is given satisfactorily by the logarithmic law. Above the transition, the situation is less clear, but the expansion coefficient appears to fit a power law better (Figure 12 and 14). The previous discussion warns against the extrapolation of the power law determined in the reduced temperature interval 10^{-2} - 10^{-1}. Hence, we use the logarithmic form for the purpose of making comparisons with the specific heat in the asymptotic limit.

A comparison of the results of the logarithmic fit given in Table 3 with the critical-region specific heat measurements of Miedema, et al.,[20] leads to two conclusions:

1. In the critical region, the specific heat is not proportional to the linear expansion coefficient. Therefore, the nearest and second-nearest neighbor spin correlation functions do not have the same temperature dependence throughout this region, and the exchange constants do not have the same stress dependence.

2. The shift of the Curie point with stress can be calculated using the ratio between the asymptotic terms in the expansion coefficient and the specific heat. We find

$$\left(\frac{\partial T_c}{\partial \sigma_1}\right)_{\sigma_{j/1}} = -(1.53 \pm 0.05)\times 10^{-11}\text{K cm}^2/\text{dyne},$$

where the subscript refers to the a direction. This result agrees within experimental error with the value found above from different considerations.

Unfortunately, there is not sufficient information to evaluate the strain dependence of the transition temperature. The moduli of compliance are not known. Although the stress dependence of the Curie point is the same for the b direction as the a direction, we cannot determine this quantity for the c direction without performing another series of measurements. To estimate a value for the elastic moduli, assume isotropic behavior so that

$$s_{ii} = \left(\frac{\partial e_i}{\partial \sigma_i}\right)_{\sigma_{j/i},T} \simeq K/3,$$

where we use the compressibility of alum as discussed in Chapter II.

Then Eq. [10] of Chapter II gives

$$\frac{1}{T_c}\left(\frac{\partial T_c}{\partial e_1}\right)_{\sigma_{j/1},T} \simeq 7,$$

where the subscript 1 indicates the a axis. If we further assume all $\frac{\partial T_c}{\partial e}$ are equal for i = 1,...,3, we find as an order-of-magnitude value,

$$\frac{d \log T_c}{d \log V} \sim 7/3.$$

Considering the assumptions made, this comes quite close to the value -10/3 Bloch[35] has found for many systems coupled by superexchange.

Summary of Conclusions

Wood and Dalton have compared several critical properties of $CuK_2Cl_4 \cdot 2H_2O$ with the results of exact series and Pade approximant extrapolations above the transition and non-interacting spin-wave theory at low temperatures. They find that the salt is a close approximation to a bcc ferromagnet with first- and second-nearest neighbor Heisenberg interactions with spin 1/2.

The thermodynamics of the lambda transition shows that the thermal expansion coefficient is linearly related to the specific heat in the critical region. This is consistent with our observations. Furthermore, the shift of the Curie point with stress can be calculated using the ratio between the asymptotic terms in the expansion coefficient and the specific heat. We find

$$\frac{\partial T_c}{\partial \sigma} = (1.53 \pm 0.05)\mathrm{x}10^{-11}\mathrm{K\ cm^2/dyne}$$

for stress in the a direction.

The procedure of Callen and Callen[19] treats all single-ion crystal field effects and two-ion interactions. The expansion coefficient is given entirely by the temperature derivative of three types of spin correlation functions. When this procedure is applied to $CuK_2Cl_4 \cdot 2H_2O$, the only contributing correlation functions are $< S_1 \cdot S_2 >$ and $< S_1 \cdot S_3 >$, the nearest and second-nearest neighbor isotropic spin correlation functions, respectively. The specific heat is described by the same two functions.

In the critical region, the specific heat is not proportional to the observed linear expansion coefficient. Therefore, the two spin correlation functions do not have the same temperature derivative and the two exchange constants do not have the same stress dependence. The stress dependence of the exchange constants is expected to be only a very weak function of temperature, so the latter result should hold for all temperatures below 4 K.

Our measurements suggest the expansion coefficient is proportional to the specific heat above 1.5 K. Therefore, the two exchange constants have the same stress dependence and/or the two spin correlation functions have proportional temperature derivatives. Measurements in the critical region suggest the former is not true, so this result supports the cluster approximation method applied to the problem of first- and second-nearest neighbor Heisenberg interactions with spin 1/2 which predicts the two spin correlation functions have equal temperature derivatives above the critical region.

Furthermore, assuming equality of the temperature derivatives of the two spin correlation functions, one can calculate the stress dependence of the transition temperature from the ratio of the expansion coefficient to the specific heat.

The result is given by

$$\frac{\partial T_c}{\partial \sigma} = -(1.40 \pm 0.09) \times 10^{-11} \mathrm{K\ cm^2/dyne}$$

for stress in the a direction. This is equal within experimental error to the value found in the critical region from entirely different considerations.

REFERENCES

1. L. P. Kadanoff, W. Götze, D. Hamblen, R. Hecht, A. E. S. Lewis, V. V. Palciauskas, M. Rayl, J. Swift, D. Aspnes, and J. Kane, Rev. Mod. Phys. 39, 395 (1967).

2. K. Huang, Statistical Mechanics (John Wiley and Sons, New York, 1963), p. 335.

3. W. P. Wolf, M. J. M. Leask, B. Mangum, and A. F. G. Wyatt, Proc. Int. Conf. Magnetism, Kyoto, Japan 1, 158 (1961).

4. A. H. Cooke, D. T. Edmond, C. B. P. Finn, and W. P. Wolf, Proc. Int. Conf. Magnetism, Kyoto, Japan 1, 157 (1961).

5. J. F. Dillon, Jr., J. Appl. Phys. 33, 1191S (1962).

6. I. Tsubokawara, J. Phys. Soc. Jap. 15, 1661 (1960).

7. B. T. Matthias, R. M. Bozorth, and J. H. Van Vleck, Phys. Rev. Letts. 7, 160 (1961).

8. G. Busch, P. Junod. M. Risi, and O. Vogt, Report of the International Conference on Physics of Semiconductors, Exeter 1962 (The Institute of Physics and the Physical Society, London, 1962).

9. T. R. McGuire, B. E. Argyle, M. W. Shafer, and J. S. Smart, J. Appl. Phys. 34, 1345 (1963).

10. S. H. Charap and E. L. Boyd, Phys. Rev. 133, A811 (1964).

11. P. Heller and G. B. Benedek, Phys. Rev. Letts. 14, 71 (1965).

12. J. F. Dillon, Jr. and C. E. Olsen, Phys. Rev. 135, A434 (1964).

13. J. Callaway and D. C. McCollum, Jr., Phys. Rev. 130, 1741 (1963).

14. V. L. Moruzzi and D. T. Teaney, Solid State Comm. 1, 127 (1963).

15. D. T. Teaney in Proceedings of the Conference on Phenomena in the Neighborhood of Critical Points, edited by M. S. Green and J. V. Sengers (NBS miscellaneous publication 273, Washington, D.C., 1966) p. 50.

16. V. L. Moruzzi, D. T. Teaney, and C. F. Guerci, Bull. Am. Phys. Soc. 12, 133 (1967).

17. B. E. Argyle, N. Miyata, and T. D. Schultz, Phys. Rev. 160, 413 (1967).

18. B. E. Argyle and N. Miyata, Phys. Rev. 171, 555 (1968).

19. H. B. Callen and E. Callen, Phys. Rev. 136, A1675 (1964).

20. A. R. Miedema, R. F. Wielinga, W. J. Huiskamp, Physica 31, 1585 (1965).

21. A. R. Miedema, H. Van Kempen, and W. J. Huiskamp, Physica 29, 1266 (1963).

22. I. Itoh, M. Fujimoto,and H. Ibamoto, Phys. Rev. 83, 852 (1951).

23. H. Suzuki and T. Watanabe, Phys. Letts. 26A, 103 (1967).

24. L. Chrobak, Z. Krist. 88, 34 (1935).

25. R. W. G. Wyckoff, Crystal Structures, Vol. 3 (Interscience Publishers, New York, 1948).

26. H. Abe, K. Ono, I. Hayashi, J. Shimada, and K. Iwanaga, J. Phys Soc. Jap. 9, 814 (1954).

27. N. C. Ford, Jr., and C. D. Jeffries, Phys. Rev. 141, 381 (1966).

28. H. Abe, H. Morigaki, and K. Koga, Phys. Rev. Letts. 9, 338 (1962).

29. H. Kumagai, H. Abe., J. Schimada, I. Hayashi, K. Ono, and H. Ibamoto, J. Phys. Soc. Jap. 7, 535 (1952).

30. K. Ono, H. Abe, and J. Shimada, Phys. Rev. 92, 551 (1953).

31. K. Ono, and M. Ohtsuka, J. Phys. Soc. Jap. 13, 206 (1958).

32. J. Van den Broek, L. C. Van der Marel, and C. J. Gorter, Physica 27, 661 (1961).

33. D. W. Wood and N. W. Dalton, Proc. Phys. Soc. (London) 87, 755 (1966).

34. G. K. White, Proc. Roy. Soc. (London) A286, 204 (1965).

35. D. Bloch, J. Phys. Chem. Solids 27, 881 (1966).

36. P. Heller and G. B. Benedek, Phys. Rev. Letts. 8 428 (1962).

37. T. Yamamoto, O. Tanimoto, Y. Yasuda, and K. Okada, in Proceedings of the Conference on Phenomena in the Neighborhood of Critical Points, edited by M. S. Green and J. V. Sengers (NBS miscellaneous publication 273, Washington, D. C., 1966), p. 86.

38. F. J. Cadieu and D. H. Douglass, Jr., Phys. Rev. Letts. 21, 680 (1968).

39. C. Domb, Proc. Phys. Soc. (London) 86, 933 (1965).

40. C. Domb, Proc. Phys. Soc. (London) 88, 260 (1966).

41. P. W. Anderson, Phys. Rev. 115, 2 (1959).

42. P. W. Anderson, in Solid State Physics, Vol. 14, edited by F. Seitz and D. Turnbull (Academic Press, N. Y., 1963) p. 99.

43. P. W. Anderson, in Magnetism, Vol. 1., edited by G. T. Rado and H. Suhl (Academic Press, N. Y., 1963), p. 25.

44. E. Callen and H. B. Callen, Phys. Rev. 139, A455 (1965).

45. H. B. Huntington, in Solid State Physics, Vol. 7, edited by F. Seitz and D. Turnbull (Academic Press, N. Y., 1958), p. 214.

46. K. S. Aleksandrov and T. V. Ryzhova, Soviet Physics-Crystallography 6, 228 (1961).

47. O. K. Rice, J. Chem. Phys. 22, 1935 (1954).

48. V. Janovec, J. Chem. Phys. 45, 1874 (1966).

49. M. J. Buckingham, and W. M. Fairbank, in Progress in Low Temperature Physics, Vol. 3, edited by C. J. Gorter (North-Holland Publishing Company, Amsterdam, 1961), p. 80.

50. J. W. Philp, R. Gonano, and E. D. Adams, J. Appl. Phys. 40, 1275 (1969).

51. J. H. Van Vleck, J. Chem. Phys., 5, 320 (1937).

52. C. Domb, in Magnetism, Vol. 2A, edited by G. T. Rado and H. Suhl (Academic Press, N. Y., 1965), p. 1.

53. G. A. Baker, Jr., H. E. Gilbert, J. Eve, and G. S. Rushbrooke, Phys. Rev. 164, 800 (1967).

54. P. J. Walsh, M. S. Thesis, University of Florida (1963).

55. G. C. Straty, Ph.D. Dissertation, University of Florida (1967).

56. T. R. Roberts and S. G. Sydoriak, Phys. Rev. 102, 304 (1956).

57. S. G. Sydoriak and T. R. Roberts, Phys. Rev. 106, 175 (1957).

58. J. G. Collins and G. K. White, in Progress in Low Temperature Physics, Vol. 4, edited by C. J. Gorter (North-Holland Publishing Company, Amsterdam, 1964), p. 450.

59. C. A. Swenson, to be published in Proceedings of the 1968 Symposium on Thermal Expansion in Solids.

60. K. Andres, Cryogenics 2, 93 (1961).

61. P. W. Sparks and C. A. Swenson, Phys. Rev. 163, 779 (1967).

62. J. F. Jarvis, D. Ramm, and H. Meyer, Phys. Rev. 170, 320 (1968).

63. G. C. Straty and E. D. Adams, Phys. Rev. 169, 232 (1968).

64. G. K. White, Cryogenics 1, 151 (1961).

65. A. M. Thompson, I. R. E. Transactions on Instrumentation, I-7, 245 (1958).

66. J. C. Maxwell, A Treatise on Electricity and Magnetism Vol. 1, (Dover Publications, Inc., N. Y., 1954), p. 308.

67. R. H. Carr and C. A. Swenson, Cryogenics 4, 76 (1964).

68. B. E. Keen, D. P. Landau, and W. P. Wolf, J. Appl. Phys. 38, 967 (1967).

BIOGRAPHICAL SKETCH

Joseph Wesley Philp was born February 19, 1944, at Stuart, Florida. He received his elementary and high school education there and graduated Valedictorian from Martin County High School in June, 1962. Entering the University of Florida in September, 1962, he received the degree of Bachelor of Science (with honors) in April, 1965. He then enrolled in the Graduate School of the University of Florida, where he received the degree of Master of Science in April, 1967. Since that time he has pursued his work toward the degree of Doctor of Philosophy.

He was awarded a Graduate School Fellowship in September, 1965, and has been a NASA Trainee since September, 1966.

Joseph Wesley Philp is married to the former Lyla Arleen Stanford. He is a member of Sigma Pi Sigma and Phi Beta Kappa.

This dissertation was prepared under the direction of the chairman of the candidate's supervisory committee and has been approved by all members of that committee. It was submitted to the Dean of the College of Arts and Sciences and to the Graduate Council, and was approved as partial fulfillment of the requirements for the degree of Doctor of Philosophy.

August, 1969

E. Ruffin Jones

Dean, College of Arts & Sciences

Dean, Graduate School

Supervisory Committee:

E. D. Adams

Chairman

J. A. Scott

C A Hooper

James B. Conklin Jr.

Ludvik Jarvis